A THESIS

FOR THE DEGREE OF DOCTOR OF PHILOSOPHY

All-Printed Antennas Based on Transparent Substrates for RF Electronic Devices

Arshad Hassan

Department of Ocean System Engineering

GRADUATE SCHOOL

JEJU NATIONAL UNIVERSITY

December, 2017

All-Printed Antennas Based on Transparent Substrates for RF Electronic Devices

Arshad Hassan

(Supervised by Professor Jinho Bae)

A thesis submitted in partial fulfillment of the requirement for the degree of Doctor of Philosophy

2017. 12

The thesis has been examined and approved.

.....

Thesis director, Dong-Guk Paeng, Professor, Department of Ocean System Engineering

.....

Jinho Bae, Professor, Department of Ocean System Engineering

.....

Yang-Hoi Doh, Professor, Department of Electronic Engineering

.....

Yoon Hyeok Bae, Professor, Department of Ocean System Engineering

.....

Woo Young Kim, Professor, Department of Electronic Engineering

.....

Date

Department of Ocean System Engineering
GRADUATE SCHOOL
JEJU NATIONAL UNIVERSITY
REPUBLIC OF KOREA

To

My Parents and Family

Knowledge exists potentially in the human soul like the seed in the soil; by learning the potential becomes actual.

Al-Ghazali (1058-1111)

Acknowledgements

In the name of ALLAH, the Most Gracious, the Most Merciful. I would like to express my humble gratitude to Almighty ALLAH. HIS help and support is always with me and without HIS help i would not able to complete this thesis. HE bestowed me courage, patience and skills to complete the doctoral studies with ease and gratification. I would like to praise Almighty ALLAH as HE blessed me with humble Father and loving Mother. It's truly a blessing having them in my life. Almighty ALLAH bless you both for being such loving parents. I am grateful to them for their eternal love, prayers, sacrifice and every kind of support throughout my life. Especially, i am indebted to my mother who has been extremely understanding, supportive and source of inspiration.

I learnt a lot during my stay in Ocean Information System Engineering (OISE) lab because the day i joined the lab, i was just familiar with research work but now, i can exercise my potential with full confidence in research for the welfare of human beings. This is all about guidance and schooling of my supervisor Prof. Jinho Bae. So, i would like to pay my thanks and best regards to Prof. Jinho Bae who put his energy and efforts to polish my research skills with innovative thoughts and ideas. I am thankful because his advice, support, trust, motivation and encouragement from the start to the end of my Ph.D. and also he played a vital role in the completion of this thesis work. I would also like to say thank to Prof. Jinho Bae gave me confidence and provided me shelter against all kind of crisis from morally depraved conditions to financial problems during my Ph.D. studies. I am also thankful to Prof. Chong Hyun Lee who gave valuable research guidance, ideas, pleasant environment and full access to his prestige laboratory to pursue the fruitful end of my research work.

I would like to pay my gratitude to my friend Dr. Shawkat Ali who introduced me to my supervisor Prof. Jinho Bae for postgraduate studies at OSE Lab, Jeju National University. I am grateful to Dr. Qasim Zeeshan Ahmed my advisor during master's studies at National University of Computer and Emerging Sciences (FAST), Islamabad, Pakistan who encourage me to pursue my higher studies.

I would love to pay my sincere tribute to my caring and loving Sisters and Brother (Ameer AbduLLAH Khan). I am grateful to my wife for her exceptional love and prayers. I would like to extend my gratitude to my wife for taking caring of our blessed and lovely Son (Adil Khanzada). I feel sorry for my son who was neglected during my Ph.D. studies. I hope, i would make up for the time he spent without me in future. All of my family has always been a source of aspiration and admiration throughout my life either in my professional career or student life. Almighty Allah bestowed me such a noble and dominating figures in my life, without whom I could not have predicted myself to accomplish this task.

I really enjoyed the company of my colleagues at OISE lab and friends in Jeju National University. They provided such a lovely, pleasant and homely environment during my stay at Jeju National University. Few of the names are coming in my mind including Dr. Shawkat Ali, Gul Hassan, Irshad Ali, Umair, Waseem Abbas, Fasihullah, Asim Raza, Mamoon, Israr Ahmed, Dr. Shahid, Dr. Afaq, Kyani shab, Dr. Kamran Ali, Dr. Rasheed, Abdul Wahid, Dr. Jael Lee, Dr. Juhoo Kim, Kibae, Jhunhwa, Yuan Choi, Hansoo Kim, Mansoo, Younsang, Adeel, Muqeet, Fayaz, Jahanzeb, Mutee, Tahir, Imran, Dr. Zahid, Zubair and Dr. Farrukh. I would also like to thank my colleagues at NUCES-FAST Islamabad for their encouragement to pursue my Ph.D. studies which are: Dr. Waseem Ikram, Dr. Mukhtarullah, Dr. Ataul Aziz, Dr. Saeed, Aamir Munir, Rashid Karim, Ibrar Khan, Shibli Nisar, Waqas bin Abbas, Shehzad Ahmed and Niaz Ahmed.

In the end, I would like to acknowledge and promise myself to acquire wisdom with the help and blessing of Almighty ALLAH.

Arshad Hassan

Abbreviations and Notations

EHD	Electrohydrodynamic
2G	Second Generation Cell-Phone Technology
3G	Third Generation Cell-Phone Technology
LTE	Long Term Evolution
FESEM	Field Emission Scanning Electron Microscope
RF	Radio Frequency
2D	Two Dimensional
3D	Three Dimensional
DMP	Dimatix Material Printer
HFSS	High Frequency Structure Simulator
ITO	Indium Tin Oxide
PET	Polyethylene Terephthalate
OTFTs	Organic Thin Film Transistors
SNP	Silver Nano Particles
PDMS	Polydimethylsiloxane
LEDs	Light Emitting Diodes
OLEDs	Organic Light Emitting Diodes
R2R	Roll to Roll
DoD	Demand on Drop
RFID	Radio Frequency Identifications
GPS	Global Positioning System
NFC	Near Field Communications
UV	Ultra Violet
CAD	Computer Aided Design
VNA	Vector Network Analyzer
CPW	Coplanar Waveguide
DDM	Dimatix Drop Manager
AUT	Antenna Under Test
SMA	Sub Miniature Version A
NI	National Instruments
ISM	Industrial, Scientific and Medical band
LPDA	Log-Periodic Dipole Array

UHF	Ultra High Frequency
FTO	Fluorine doped Oxide
DC	Direct Current
PSI	Phase Shifting Interferometry
Wi-Fi	Wireless Fidelity
SOL	Short-Open-Load
HP	Hewlett Packard
FR-4	Flame Retardant 4
dBi	Decibels referenced to Isotropic gain
S_{11}	Reflection Coefficient
ε_{reff}	Effective Dielectric Constant
C	Capacitance
ε_r	Dielectric Constant
f_r	Resonance Frequency
c_0	Speed of Light
L	Inductance
R	Resistance
Z_0	Characteristic Impedance
λ	Wavelength
i	Electric Current
q	Electric Charge
v	Voltage
L_b	Bent Inductance
C_b	Bent Capacitance

List of Figures

List of Tables

List of Content

Abstract

In future, flexible electronic devices requires connectivity on Bluetooth, WLAN, 2G, 3G and 4G-LTE standards and need support of printed flexible single and multiband antennas. Therefore, flexible and bendable antennas are necessary and unavoidable. The nature of flexible technologies dictates that the antenna should be flexible as well as mechanically robust such that it can tolerate high level of bending, rolling and flexing repeatedly. These challenges should be addressed because the performance of printed antennas degrades due to deformation in the flexible substrate under severe conditions. Therefore, it is critical and important to study and analyze the printed antennas for flexible electronic devices.

The printed antennas can act as a radio frequency (RF) sensor to measure the permittivity of the liquids which can significantly detect the materials so, it is also important to analyze these printed antenna designs for RF sensors.

To address future challenges of flexible antennas, this thesis presents various single and dual band flexible printed antennas on transparent substrates with different geometries for wearable electronic devices. In last decade, printing technologies such as screen printing, electrohydrodynamic (EHD) and inkjet printing are attractive pattering techniques which are gaining much interest for mass fabrication of various wearable electronics devices. The tremendous interest in these technologies is due to their features of one-step manufacturing process and vacuum free processing that fulfills the realization of eco-friendly, low-cost and flexible electronic devices and systems. New organic and inorganic solution processed materials are improving the performance of the electronic devices. By utilizing the solution process materials and printing technologies, this thesis addresses the challenges of flexible antennas and RF sensor on transparent substrates.

Initially, a flexible single band monopole antenna design is presented for 1.8 GHz applications. The design of single band antenna is 2D projection of 3D helical antenna with a single turn as the 3D structures cannot be embedded in 2D flexible substrate. The mathematical modeling of the single band antenna design is presented. By using transmission line theory, the circuit model is presented which endorses the design of single band antenna and well matched with the simulation results in both circuit and

full-wave electromagnetic software simulations. The straight and bent configurations performance analysis is carried out to optimize the design, and comparative analysis with other reported antennas is also presented. To confirm the reception capability of single band antenna, it was characterized on spectrum analyzer which showed the reception of single desired band. The antenna worked well and fully operational during flexibility test as the measured reflection coefficient was under -10 dB.

A dual-band antenna design is described on a thin flexible and transparent Polyethylene Terephthalate (PET) substrate and characterized for wearable RF electronic applications. For printing both single and dual band antennas, the conductive ink based on Silver Nano Particles (SNPs) is utilized. The flexible antenna was fabricated on a very thin 40 micron substrate through inkjet material printer. To fabricate an optimal antenna on a thin substrate, the systematic procedure is given in detail. The results of fabrication process are confirmed through surface characterizations of the fabricated antenna.

Next, a flexible and transparent inset-microstrip patch antenna based on conductive indium tin oxide (ITO) is presented. The patch antenna is fabricated on a Polydimethylsiloxane (PDMS) substrate and characterized with the help of Agilent network analyzer. The bendability and transparency tests are given for transparent wearable RF electronic applications. The presented flexible antenna design shows excellent performance over the considered band. Therefore, the proposed design provides an RF industrial solutions for future low-cost, eco-friendly and flexible wearable electronic market.

Finally, a microstrip patch RF sensor is demonstrated for liquid identification. The relationship between the dielectric constant and resonance frequency provides the liquid sensing mechanism. The design procedure is given to find not only maximum frequency separation between two adjacent resonance frequencies but also lowest reflection coefficients at the resonance frequencies for all considered liquids. The fabricated sensor has 140 MHz minimum frequency separation and maximum -29 dB reflection coefficient, which gives large identification margin. By comparing with the existing sensors, the RF liquid sensor exhibits outstanding identification capability. Therefore, this type of patch sensor can be utilized in RF tunable liquid detection applications.

Chapter-1 Introduction

1.1 Background

Antenna technology is used in many electronic applications such as Wireless Fidelity (Wi-Fi), Bluetooth, Zig-bee, mobile phones, satellite communication, Radio Frequency Identification (RFID), Global Positioning System (GPS) and telemedicine radio, to facilitate the daily life. An important category in antenna technology is flexible and wearable antennas which have gained more attention from both industry and academia. The popularity and demand of flexible antennas increased because of recent advancement in the field of printed electronics. In recent years, the printed electronics has emerged as a new branch of electronics where functional materials are directly deposited through numerous printing techniques on inexpensive flexible plastic films or substrates, to make operational electronic devices and systems [1]. The electronics market analysis indicated that the estimated revenue of printed electronics is going to be 30 billion US dollars and, it will increase above 300 billion US dollars by the end of 2028 [2].

This tremendous amount of market share shows the demand and popularity of printed electronic. Consistently, the flexible electronics systems and devices often needs the integration of flexible antennas operating in the desired frequency bands to provide wireless connectivity. However, the new electronic applications impose severe limitations to meet their demands, especially which requires mechanical flexibility and compatibility with flexible electronic circuits and systems. Conventional manufacturing techniques comprises on vacuum processing and a series of thin layer film deposition steps such as coating, photoresist, etching and again photoresist peel off to transfer the pattern on the thin film. This process also involves a large waste of materials that increases the overall processing and device cost. On contrary, we can fabricate the low cost electronic devices by utilizing techniques such as inkjet, gravure and offset printing which deposit the right amount of material on the required place and there is no wastage of material in fabrication process. Furthermore, it fulfills the missing gaps of conventional lithographic process with environmental friendly, low

temperature and ambient conditions processing. Printing industry that involves offset, inkjet printing and Roll to Roll (R2R) printing processes have shown extremely fast printing of electronic circuit as meters per minute that is almost competitive to the vacuum based fabrication techniques [3].

The flexible antennas can be fabricated by using flexible polymer, plastics, polyester, polyethylene and paper as a substrate and conductive solution processed materials as an active material [4]. The substrates are low-cost, energy efficient, lightweight and compatible with large area manufacturing by utilizing R2R and also small area development is possible through sheet-to-sheet fabrication technique [5]. These substrates are the perfect complement to be used with printing technologies, rather than with standard clean-room techniques such as photolithography, lift-off or etching. From this point of view, the term flexible printed antennas often implies the use of a plastic, textile or paper substrate. In short, all the advantages of printed techniques over conventional manufacturing techniques make the flexible antenna as an attractive candidate for the future consumer Radio Frequency (RF) electronic market. Some of the printed antennas are shown in Figure 1.1.

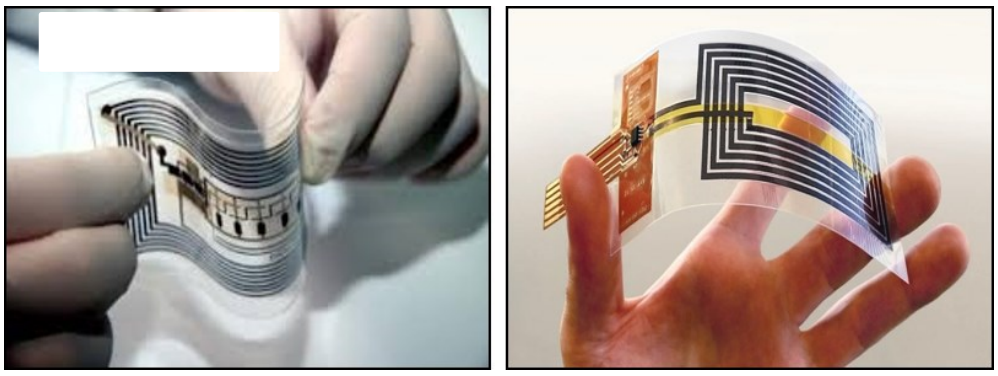

Figure 1.1. Printed flexible antennas [5], [6].

1.2 Evolution in Printed Antennas

Previously, the antennas were printed on a rigid Flame Resistance-4 (FR4) substrate to provide the wireless connectivity to the printed circuits and systems [7]. However, flexible electronics technology is one of the popular trends in modern world. To provide wireless connectively in specific frequency band over wireless networks, the vast majority of flexible electronic circuits and systems need integration of flexible

antennas. This is the necessity of today's information oriented society. The efficiency and performance of the printed electronic systems depends on the efficiency of the integrated antenna. Hence, the desired flexible antenna can not only capable of meeting the flexible wireless connectivity demands such as low-cost, compact, lightweight, low profile and mechanically robust but, also it should be efficient with desired bandwidth and radiation characteristics. To design a high functional flexible printed antenna particularly for small devices is challenging task because of its integration in a very compact size. A compact flexible and transparent antenna is needed for integration with future printed wearable electronics devices operating over the required frequency bands [8]. Therefore, an urgent demand for low-cost, fast, efficient, high-precision and reliable fabrication, exists. The task can be tackle by applying the printing technology for flexible antennas. The next section presents the available printing technologies for antenna fabrication.

1.3 Printing Technologies for Printed Antennas

Recent years have seen a great demand in the field of flexible printed antennas because of their light weight, environment-friendly, low-cost manufacturing and ease of fabrication. The availability of inexpensive substrates such as papers, textiles, and plastics make flexible printed antenna an attractive candidate for the next generation of consumer electronics systems. This section describes the current available printing technologies for the fabrications of wearable flexible antennas. Among these available methods, some are matured and commercialized whereas some techniques are still under research. The key task of the printing technique is to deposit the functional active materials on the flexible substrate with high accuracy and uniform film thickness.

In history, various thin films deposition techniques have been adopted that includes chemical bath, slot casting, spin-coating, spray coating, dip coating, screen printing, doctor blade, inkjet printing, metering rod and aerosol jet. Figure 1.2 shows the schematic diagrams of different printing techniques. Other printing techniques, electrostatic spray deposition (ESD) and electro hydrodynamic (EHD) are also used for the deposition of thin films, where the functional material is deposited using electrostatic field [2]. All fabrication methods have their own advantages and disadvantages.

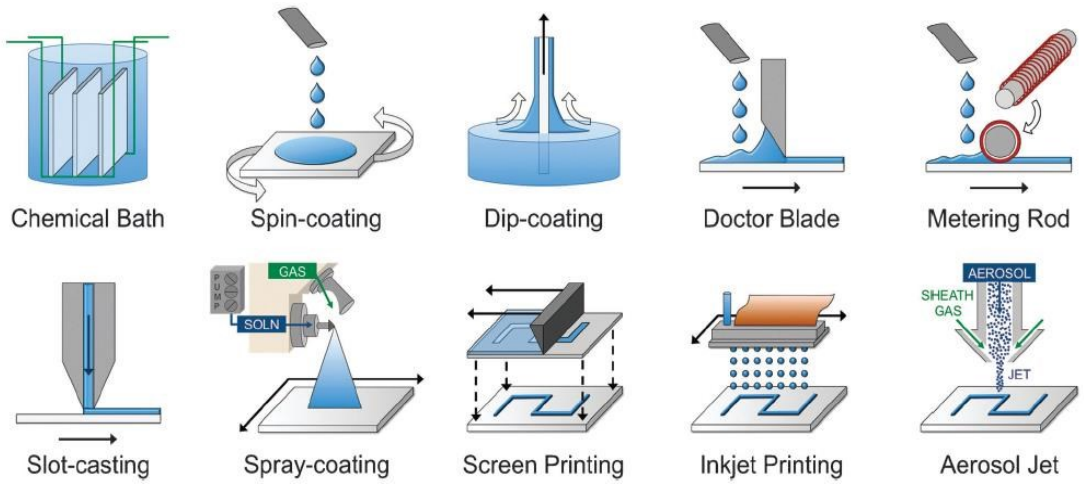

Figure 1.2. Various printing techniques based on solution-processed manufacturing [2]**Error! Reference source not found.**.

In this thesis, ink-jet printing technique is used for the fabrication of flexible antennas and RF sensor. This technique is discussed in the forthcoming section.

1.4 Inkjet Printing Technology for Antenna Printing

In this work, inkjet Digital Material Printer (DMP-3000) has been utilized for printing the antenna design. Digital photograph of the DMP-3000 is shown in the Figure 1.3 (a), it consists of a DMP-3000 printer and a personal computer with monitoring unit. Figure 1.3 (b) shows the schematic diagram of the DMP-300 printer. The main components are shown which includes temperature controller, camera, monitor, PC, nozzles head, ink reservoir, pressure controller, LED light and moveable stage. The DMP-3000 printer has print area of 300 × 300 mm, position accuracy of ±5 μm, repeatability of ±1 μm, and platen temperature in the range of 25 to 60 °C. To print a pattern of antenna through inkjet printer various steps are followed from design of layout to the device [9].

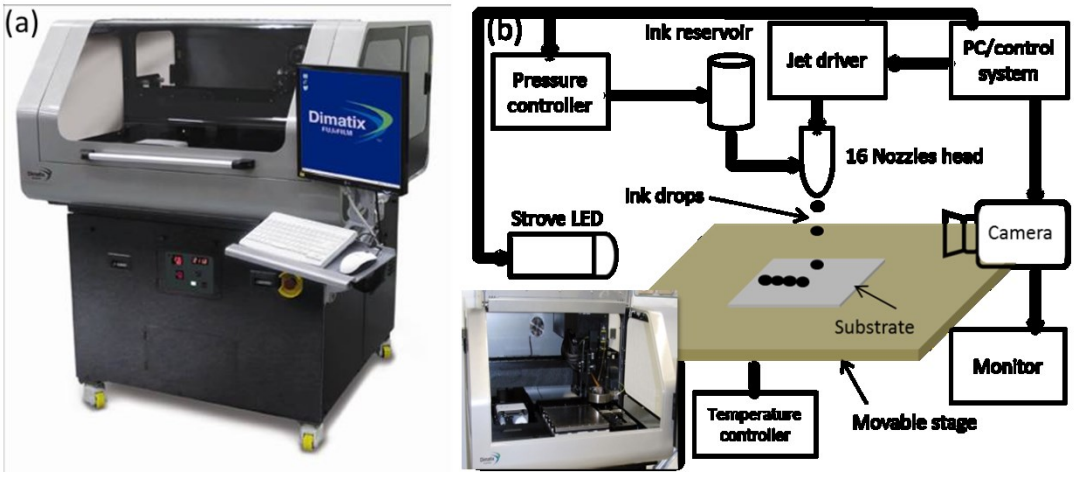

Figure 1.3. (a) Digital photograph of DMP-3000 inkjet material printer. (b) Schematic diagram of the DMP-3000 along main components [9].

1.5 Future Trends and Challenges of Printed Antennas

To meet with the demands of next generations electronic applications which are low-cost, large area, flexible and environmentally friendly, printed electronics is an attractive, appealing and emerging field. The printed electronic devices such as OLED display, RFID tags and biomedical sensors are well matured and commercialized. To communicate these flexible printed electronics devices, the integration of flexible antenna is necessary to provide wireless connectively over wireless networks. The flexible antenna should be low-cost in both materials and fabrication [5], [8].

Day by day, the demand for antennas is increasing to suit a wide variety of exciting applications such as flexible and wearable electronic sensing and wireless applications. The optimal functionality of these printed devices depends on the characteristics of the integrated antenna. The main challenge is not only to meet with the nature of requirements of printed electronics such as low-cost, flexible, compact, lightweight and environmentally friendly device but also to provide a mechanically robust and efficient solution in term of performance. The nature of flexible technologies dictates that the antenna should be flexible as well as mechanically robust such that it can tolerate high level of bending, rolling and flexing repeatedly.

There are additional challenges associated in designing the flexible antennas which do not exist when designing conventional antennas for wireless systems. The resonant frequency and return loss of the flexible antenna deteriorates and these losses should be accounted. Subsequently, flexible antennas are prone to deterioration due to

impedance mismatch under bent or rolled conditions. The functionality and efficiency of the antenna also degraded under these severe operation scenarios.

1.6 Author's Contribution and Thesis Organization

1.6.1 Contributions

The main objective of thesis is to address these challenges by presenting a systematic approach that includes the design, simulation, fabrication and characterization of Nano Particles (NPs) based antennas and sensor. Moreover, the focus of this research is to develop versatile low-cost antennas and sensor by exploring new design techniques, printing technologies and functional active materials to realize the optimized eco-friendly flexible printed antenna. In this context, the research is divided into four sections which are explored step by step. In first part, innovative 2D monopole single band design which is projection of 3D helical antenna is developed with electrical conductive Silver Nano Particles (SNPs) ink and extremely flexible thin Polyethylene Terephthalate (PET) substrate. A systematic design approach with the help of transmission line theory is presented and, the design performance is confirmed through fabricated antenna. A performance comparison of the proposed SNP-based miniature printed antenna is presented with the identical printed antennas which reveals that the presented single band monopole design has excellent performance in term of gain, efficiency, compactness and robustness. In the next part, a coplanar waveguide (CPW) based high gain dual-band monopole design is presented on a very thin 0.04 mm flexible PET substrate for both radar and communication bands. The inkjet printing process is explored and analyzed on a thin substrate through SNPs based ink. The effects of printed layer thickness and number of printed conducting layers on the performance of antenna are investigated. The effect of ultra violet treatment, curing time and temperature on SNP film is examined. The film uniformity and thickness is evaluated through 3D surface morphology and Scanning Electron Microscope (SEM). A systematic procedure is presented that yields excellent fabrication which is confirmed through flexibility test. In the third section, a low-cost flexible transparent inset microstrip antenna is developed through inkjet printing technique for transparent flexible electronic applications. To design and analyzed the indium tin oxide (ITO) and Polydimethylsiloxane (PDMS) based antenna Finite Element Method (FEM)

formulation is implemented in High Frequency Structure Simulator (HFSS). The optical and electrical measurement performed by using Shimadzu spectrophotometer and Hewlett-Packard (HP) network analyzer, respectively. The antenna showed up to 90% transparency. In the fourth and final part of this research, a low-cost inset microstrip based RF inkjet printed sensor is developed for liquid sensing applications. The FEM based best design is achieved which can easily identifies the considered liquids as the resonance frequency separation is large and reflection coefficient is under -25 dB.

1.6.2 Thesis Organization

The thesis is organized into six chapters as follows:

Chapter 2 deals with the design, equivalent circuit, working mechanism, fabrication and characterization of single band monopole antenna on a very thin 40 micron PET substrate. The FEM based analysis of the antenna design is described in detail. The antenna is fabricated by utilizing inkjet printing technique. The electrical, mechanical and surface morphological characteristics are investigated for the fabricated devices.

Chapter 3 review and describes the dual bands 900 MHz and 2.4 GHz antenna design. The working principle on both bands is done in detail. The current distributions and radiation characteristics are discussed on both operational bands. The dual band antenna design is fabricated on a very thin 40 micron PET substrate through DMP-300 inkjet material printer. The fabrication process is described in detail as it was challenging to deposit the antenna pattern of this thin hydrophobic substrate. The surface morphological, electrical and mechanically characteristics is done to show its compatibility with the wearable printed electronics applications.

Chapter 4 deals with fabrication of transparent microstrip patch antenna on a flexible and transparent PDMS substrate. The transparent and conductive ITO ink has been utilized to fabricate the patch and the ground of the antenna design. The optical transparency analysis is done that shows, the device is transparent. The electrical and mechanically performance is investigated for transparent printed wearable electronic applications.

Chapter 5 describes a printed RF inset-microstrip sensor for liquid identification applications. The full wave analysis is shown in detail to obtain the best sensor design in term of minimum reflection coefficient (for all considered liquids) and large resonance frequency separation among liquids. The Ag Nano Particles (AgNPs) ink is used to fabricate the liquid RF sensor through inkjet printing technique. The sensor performance is shown to distinguish various liquids including water, oil, ethanol and mixed cases.

Chapter 6 describes the conclusion of this thesis and future work.

Chapter-2 Single band Monopole Antenna

2.1 Introduction

Nowadays, printed electronics has gained high attention due to low cost, environment friendly, and easy fabrication of electronic devices. In particular, printed antenna is common in RFID, near field communication (NFC), high frequency radio transmission and reception applications [10-15]. Printing techniques like EHD, screen printing and inkjet are low cost and have ability to deposit the material accurately on hydrophilic material substrates [16-24]. There are some substrates which are hydrophobic (like PDMS). However, the ink can be effectively deposit on these substrates with good contact angle by utilizing a small treatment such as plasma or UV [25]. Therefore, manufacturing of printed antennas is possible without high cost wet etching processes by direct printing techniques [26]. The selection of the low cost transparent and biocompatible substrate material is important to print antenna for wearable electronics devices. Recently, printed antennas on various flexible substrates, including paper, kapton and polyimide film has been reported [27-32]. Among these substrate materials, paper is low profile (with small thickness and weight) flexible and low cost substrate which is commonly used for printing antennas in printing electronic devices [31]. However, paper based opaque substrates are not robust and cannot be used in hard ambient environment. Secondly, all these substrates are mainly restricted by their high loss tangent (such as for paper $\tan\delta = 0.072$ from 0.5 to 2.5GHz). Hence, low cost PET substrate is now used in many printed wearable electronic applications like OLEDs, organic thin film transistors (OTFTs) and organic memory [33-36], is a promising substrate with lower tan loss factor of 0.003 at 1 GHz [37]. Furthermore, the surface roughness of the PET is lower as compared to other substrate material like paper, which also lowers the reflection loss due to surface roughness of the substrate material [38]. Recently, a few antenna designs have been demonstrated on PET substrate [39-42] but most of the works have been carried out for prior RF characteristics to support printed antenna and also the printed designs are not compact [42]. To design high functional antennas particularly for small devices (like Teleos etc.) is a difficult and challenging task due to their integration in a very compact

geometry. A compact flexible and transparent antenna is needed for integration with future printed small wearable electronics devices operating over 1.8 GHz band.

To apply wearable electronics devices at 1.8 GHz band, a compact printed antenna design on a fully flexible and transparent PET substrate is presented. The proposed antenna is designed by using resonant properties of printed monopole and is a variant of monopole designs presented in [30-31], [43]. The antenna is designed and simulated in general purpose computer aided design (CAD), Ansys HFSS. The simulated design is fabricated through commercial Dimatix inkjet material printer (DMP-3000) at ambient conditions, by depositing silver nanoparticle ink on a PET substrate in single step. The fabricated antenna is electrically characterized by using vector network analyzer (VNA). The measured reflection coefficient is -32.2dB at 1.8GHz and -10dB bandwidth of 190.5MHz. The practical signal strength of -60.64 dBm is received by using LG spectrum analyzer. The simulated gain of the proposed antenna is 2.72dBi and its efficiency is 93.33%. Mechanically the propose antenna is fully flexible, and optically transparent on a 40micron PET substrate. The proposed antenna geometry is simple and can be tunable to any frequency.

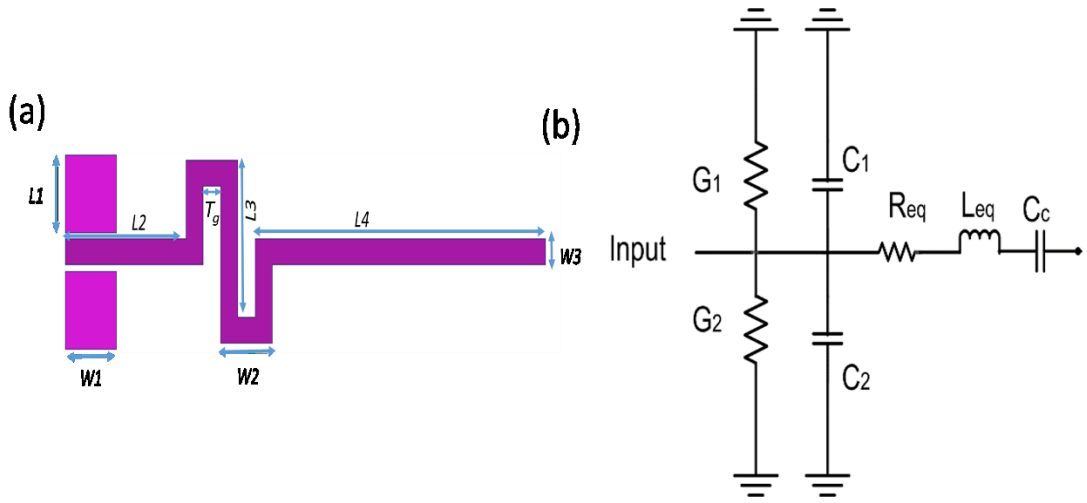

Figure 2.1. (a) Antenna design. (b) The equivalent electrical circuit of antenna.

2.2 Antenna Design

The geometry of the antenna as shown in **Figure 2.1**(a) is inspired from helical antenna. The space and number of turns in the meander pattern defines the value of inductance and capacitance [44], in this design we have used only one turn to achieve our desired

inductance and capacitance values for 1.8 GHz band. The antenna is fed by coplanar waveguide (CPW) due to its advantage of low dispersion and low radiation leakage over simple microstrip line feed method. Secondly, CPW antenna makes antenna fabrication simple and fast as the radiating element and the ground are printed on the same side of the substrate. The basic radiating element is formed by a single right angle bend as shown in the center of **Figure 2.1**(a), where most radiation occurs due to discontinuities [45]. The right angle bends are used to reduce the discontinuity susceptance which helps in impedance matching. The impact of right angled part in the antenna is acting like a load and a single turn is equivalent to an inductor. The magnetic field inside the turn is canceled out and only the horizontal parts of turns contributes in far field radiation pattern. Most of the radiation occurred at right angle bends which add up to produce desire polarization of the antenna. The considered substrate is 0.04mm thick PET whose dielectric constant is 2.8 and loss factor of 0.003 at 1GHz frequency [37]. The conductivity of silver nanoparticle ink (which is used to for radiating element) is 1.42 x 10^5 S/m after sintering at 240°C [46]. There is tradeoff between bandwidth and gain while increasing number of turns. The turn gap of 2.7mm is selected to lower the capacitive coupling between the radiating arms. Furthermore, the resonant frequency is directly proportional to the physical length of the antenna and shape. The straight elements L_2, W_4 and L_4 are sensitive to resonance frequency as they are multiple of wavelength while the transition can be adjusted.

2.2.1 Equivalent circuit design

The equivalent circuit diagram of the antenna is given in **Figure 2.1**(b). The shunt conductance G_1 & G_2 and shunt capacitances C_1 & C_2 are present between antenna feed line and ground plane through air. The silver pattern bulk resistance, inductance and capacitance are given by R_{eq}, L_{eq} and C_{eq} respectively. We explain the signal transmission from input of the antenna to the air through our antenna's equivalent circuit. Initially, a low frequency signal is applied to the antenna, the impedance of the circuit is high due to the C_{eq} as capacitances are open circuit at low frequencies ($X_C=1/2\pi fC$). In this case the signal is dropped on the circuit and do not flow to the air. On the other hand, when a high frequency signals is applied to the input of antenna, the impedance of the antenna becomes high due to the reactance of L_{eq} ($X_L= 2\pi fL$). In between there is a resonance frequency (1.8GHz) of the circuit where inductive

reactance is equal to the capacitive reactance and they cancel each other. In this case, the total impedance of the circuit is equal to the R_{eq} which indicates low impedance hence, maximum signal passes through the circuit. Using the analogy of the electrical equivalent circuit, only certain frequency band passes to the air and rest of the frequencies are reflected back to the source due to mismatch of the impedance. The proposed antenna geometry is optimized in terms of resonance frequency, gain and size as described in sections 2.2.2, 2.2.3 and 2.2.4. The geometry design has a significant impact on the performance of the antenna as described in detail in section 2. The dimensions of the proposed antenna are given in **Table 2.1**.

Table 2.1. Design parameters of antenna.

Parameter	Dimension (mm)	Parameter	Dimension (mm)
L_1	4.05	L_3	8.14
W_1	4.05	W_3	1.35
L_2	15.8	L_4	22.75
W_2	5.4	T_g	9.49

The antenna structure is a combination of straight line segments and bending segments. The line segments are considered as distributed transmission line [44], [47]. The lumped parameter equivalent for straight transmission line segments is represented by T-equivalent network as shown in **Figure 2**.2 (a) where Z_1 is defined by the following equation.

$$Z_1 = jZ_o \tan(\beta l) \tag{1}$$

Here, $= 2\pi/\lambda_{eff}$, and $\lambda_{eff} = \frac{\lambda_o}{\sqrt{\varepsilon_{eff}}}$, $\lambda_o = c/f$ and ε_{eff} is given by,

$$\varepsilon_{eff} = \frac{\epsilon_r + 1}{2} + \frac{\epsilon_r - 1}{2} \sqrt{\frac{1}{1 + \frac{12h}{w}}}$$

where ϵ_r represents the relative permittivity of the substrate and h is the height of the substrate.

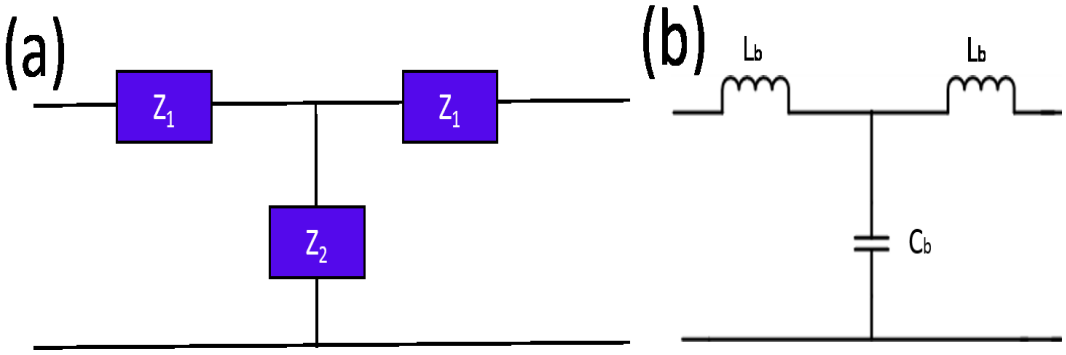

Figure 2.2. (a) Equivalent T-network. (b) Lumped model of right angle bend.

In equation (1) Z_0 represents the characteristic impedance of the transmission line and is given by the following relationship [43],

$$Z_0 = 276 \log\left(\frac{2s}{w}\right)$$

where s is the spacing between turns and w is the track width of transmission line. The second impedance Z_2 is given by the following equation,

$$Z_2 = -\frac{jZ_o}{\tan(\beta l)} \tag{2}$$

As $\tan(x) \approx x$ and $\sin(x) \approx x$ for $l \ll \lambda g$. Using this approximation Z_1 in equation (1) becomes inductive reactance as $Z_1 = jZ_o\beta l$ while Z_2 in equation (2) becomes capacitive reactance as $Z_2 = -\frac{jZ_o}{\beta l}$.

By comparing Z_1 with inductive reactance $Z_1 = j\omega Ll$ and Z_2 with capacitive reactance $Z_2 = 1/j\omega Cl$, and using Z_0 and β, yields the following expressions to calculate the inductance and capacitance (per unit length) of the straight line segments respectively.

$$L = \frac{Z_o\sqrt{\varepsilon_{eff}}}{c}$$

$$C = \frac{\sqrt{\varepsilon_{eff}}}{cZ_o}$$

The overall lumped inductance and capacitance of the structure is given by $L_1 = Ll$ and $C_1 = Cl$ respectively. Where l represents the length of line segment.

The bending line segments can be represented by T-network with inductance and capacitance as shown in **Figure 2**.2 (b). The charge accumulates at the corners (bents) which creates capacitance while, the interruption of current at the corner produce inductance. The bending inductance and capacitance is given by [48].

$$\frac{C_b}{w} = \frac{(9.5\epsilon_r + 1.25)\mathrm{w}}{h} + 5.2\epsilon_r + 7 \left[\frac{pF}{m}\right] \quad , \left[\frac{w}{h} > 1\right]$$

$$\frac{L_b}{w} = 100\left(4\sqrt{\frac{w}{h}} - 4.21\right)\left[\frac{nH}{m}\right]$$

Where C_b and L_b are bend capacitance and inductance respectively. There might be fringing field at the end of the structure but as the ground and end of the transmission separation is large. Hence, the open ended capacitance can be neglected. The overall lumped equivalent circuit is given in **Figure 2.3**.

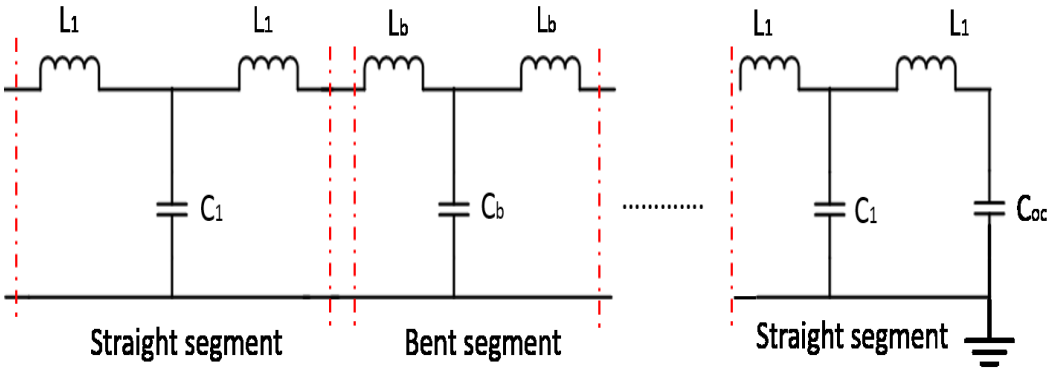

Figure 2.3. The overall lumped circuit of antenna.

2.2.2 Analysis of straight and meander designs

We have analyzed two extreme antenna designs as shown in **Figure 2.4** (a) and (b). For HFSS analysis, we used **d** as 9.49mm in **Figure 2.4** (b).

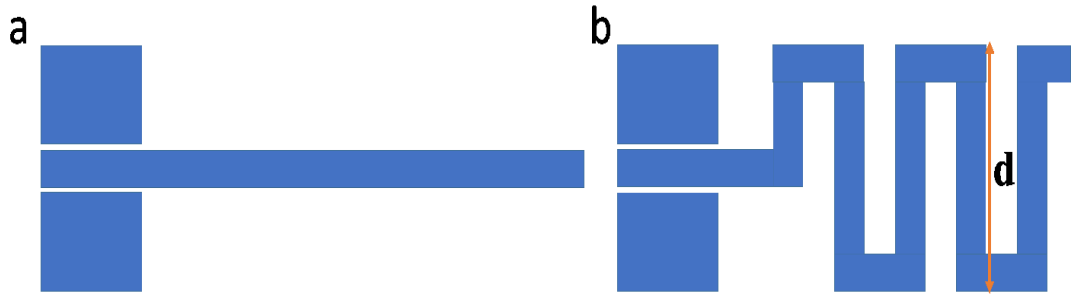

Figure 2.4. (a) Straight Geometry (b) Meander type bending geometry.

With straight design, we obtained gain of 2.5dBi and resonance frequency of 1.8GHz. With the meander design as shown in **Figure 2.5**, we obtain 3.2dBi increased gain and shifted resonant frequency of 2.55GHz. The increase of resonant frequency is due to turns (discontinuities) causing more radiations.

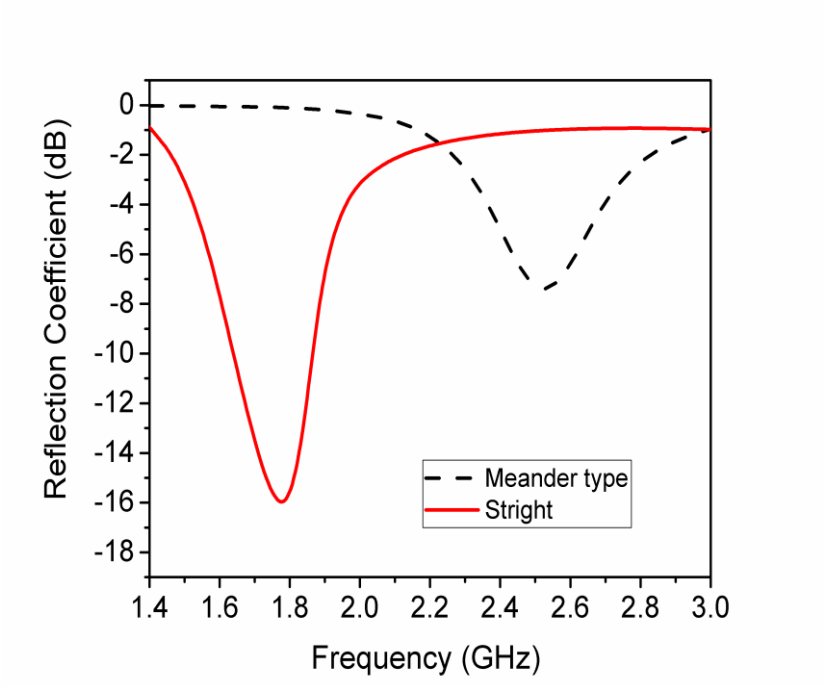

Figure 2.5. Reflection Coefficient of straight and meander type shapes

2.2.3 Analysis of right turn position variation

We analyzed antenna radiation characteristics by changing right turn position labeled as **S** in **Figure 2.6**. For analysis, we fixed **d**, height of the turn.

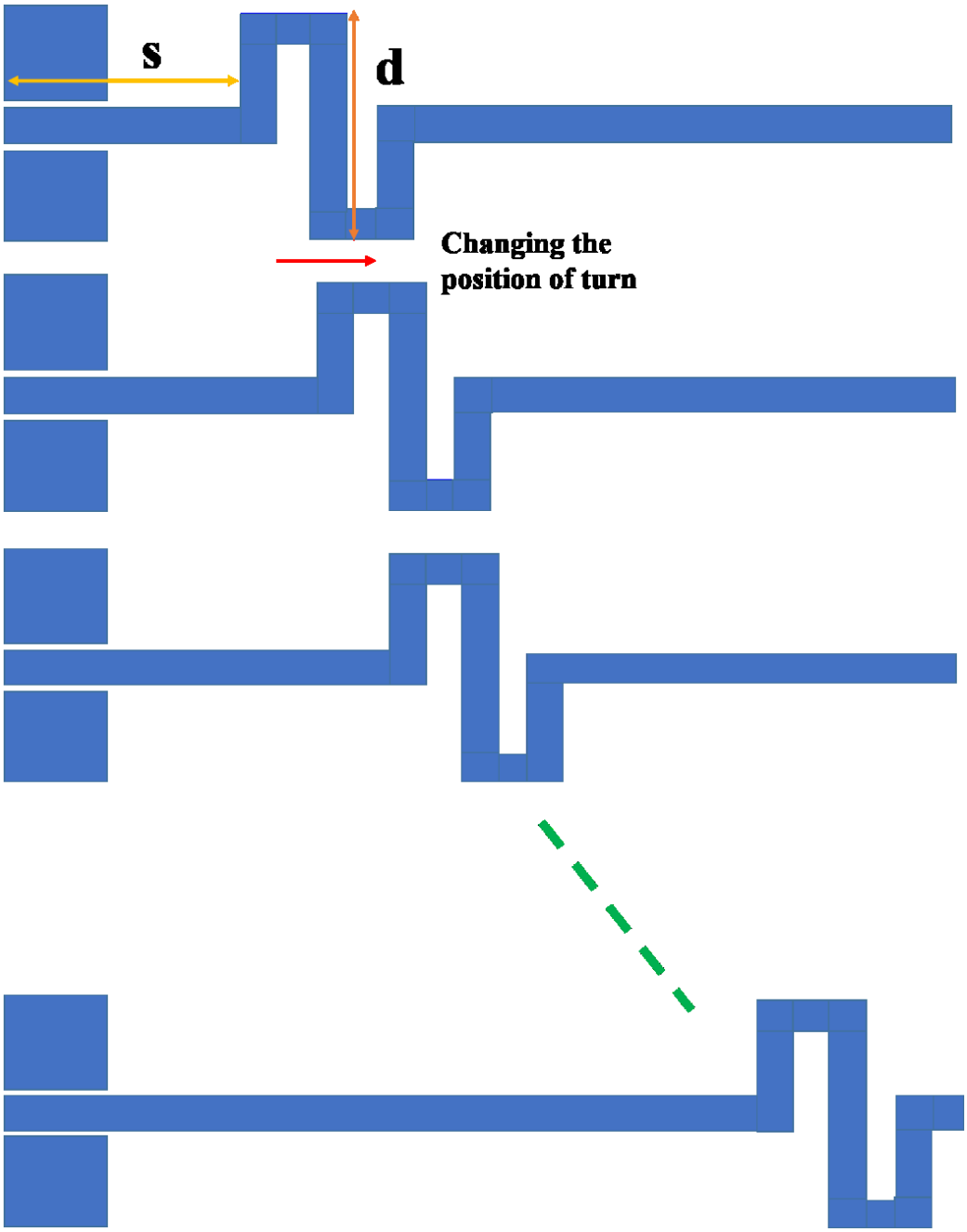

Figure 2.6. Right angle turn position variation along horizontal axis.

As shown in **Figure 2.7**, shifting the turn position near to ground causes more capacitive coupling and resonant frequency is slightly changed from 1.84GHz to lower frequency. However, shifting the turn position to right, does not cause shift of the resonance frequency of 1.84GHz and cause change of the reflection coefficient resulting in input impedance change. The maximum antenna gains at different positions of turns are summarized in **Table 2.2**.

Table 2.2. Maximum antenna gains at different turns

Parameter S [mm]	**Gain [dBi]**	**Parameter S [mm]**	**Gain [dBi]**
7.7	2.6	10.4	2.7
15.8	2.72	37	2.51

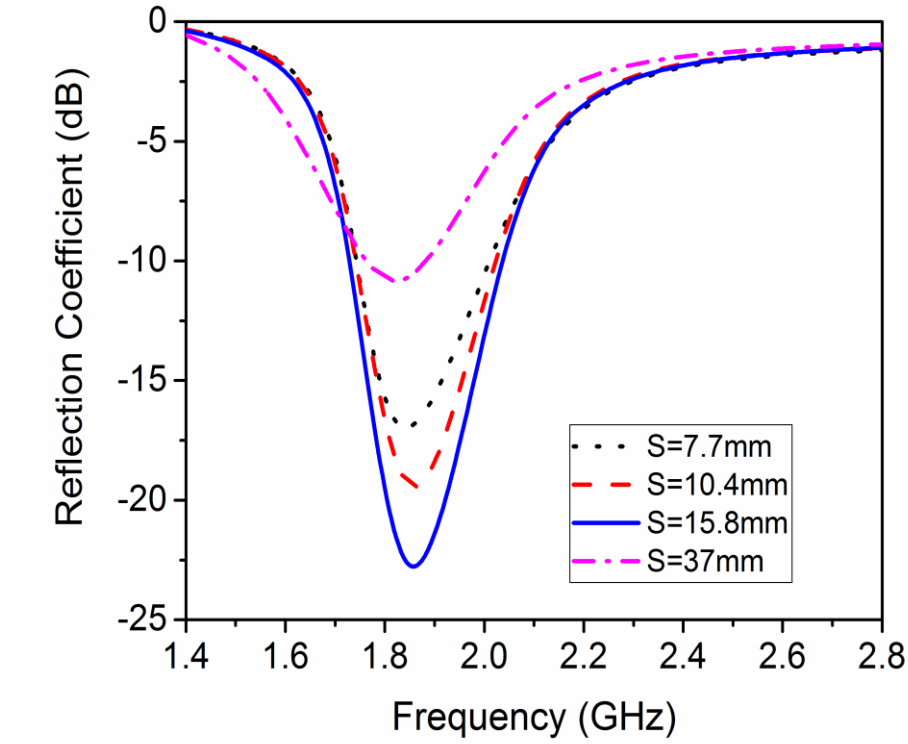

Figure 2.7. Reflection coefficients at different value of S.

2.2.4 Analysis of vertical length variation

With fixed antenna pattern length, we analyzed characteristics corresponding to variation of vertical length denoted as **d** in **Figure 2.8**. As **d** increased, antenna gain increased and the resonance frequency was changed from 1.8GHz to higher frequency as shown in **Figure 2.9**. The resonance frequency was shifted from 2.3GHz to 1.98GHz as **d** decreased from 22.5mm to 14.5mm. The maximum antenna gains against different values of **d** are given in **Table 2.3**.

Table 2.3. Maximum gains over different vertical lengths.

Parameter d [mm]	Gain [dBi]	Parameter d [mm]	Gain [dBi]
14.5	3.26	18.5	2.25
20.5	2.69	22.5	4.5

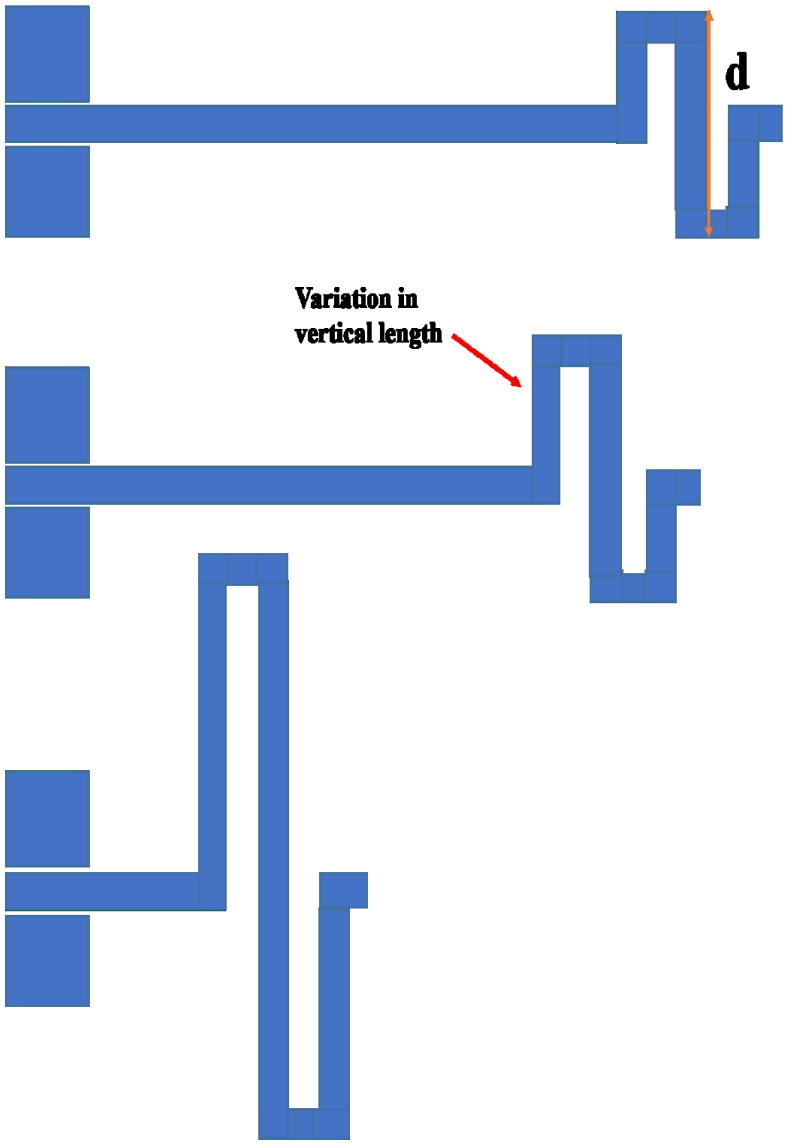

Figure 2.8. Vertical length variation of the antenna with fixed total antenna length.

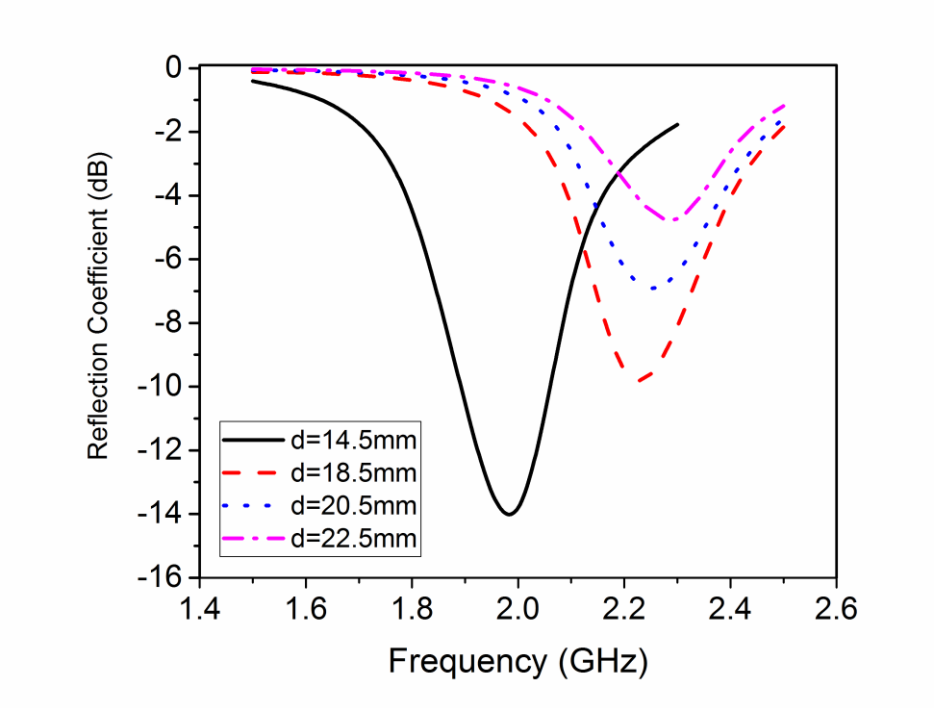

Figure 2.9. Reflection coefficient against vertical length variations.

The radiation of the antenna is highly dependent on the length of first transition and it needs to be longer enough to allow good wave conformation but increases the antenna size.

2.3 Fabrication Process

The proposed antenna was designed and simulated by HFSS and exported to ACE 3000 software that converted the design file into bitmap format with all geometrical information. Then the bitmap file was converted into Inkjet printer supported file format by Dimatix Drop Manager (DDM). Before initialization of printing process, silver nano particles ink (3ml), purchased from ANP South Korea, was filled into cartridge of 16 nozzles with diameter of 50µm and distance between nozzles is 254µm. Single drop of 10pl is selected for printing the proposed antenna pattern on a commercial 40-micron thick, flexible and transparent PET substrate purchased from sigma Aldrich. The low-cost PET substrate has good mechanical and thermal characteristics in polyamides and it can withstand up to 200 °C. Prior to printing, we cleaned the PET with ethanol at ambient conditions and then rinsing with distilled water and dry it at 50°C for 5 min, to remove scratches and contamination on the PET surface. Then we deposited the antenna pattern over the PET substrate. Due to

hydrophobic nature of the substrate, the silver nanoparticle ink was scattered over the PET surface. To resolve spreading and scattering of silver ink on the surface, experimentally we obtained that UV treatment of 30s produces optimum result. This process makes the substrate surface slightly rough and avoids random spread of silver nanoparticles over the surface. Finally, the UV treated PET was placed onto the plate of material inkjet printer, as shown in **Figure 2.10** for printing antenna pattern.

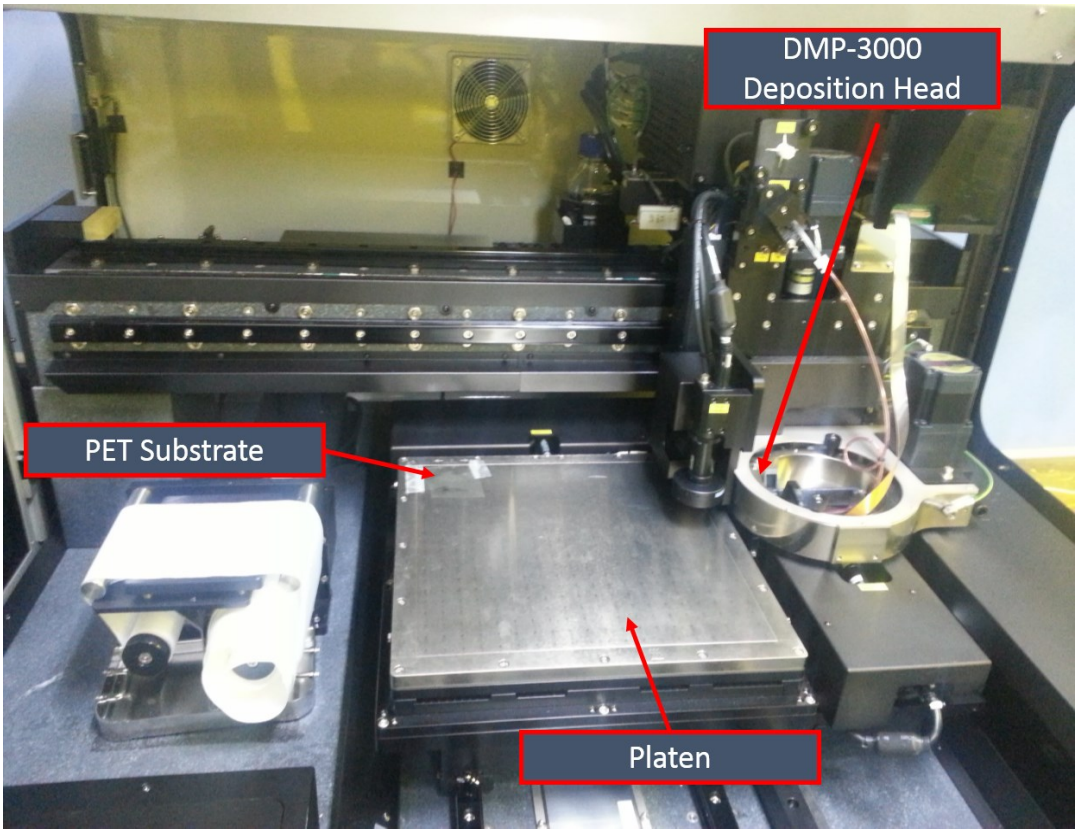

Figure 2.10. Direct printing of the antenna on PET substrate using Dimatix Inkjet Material Printer.

The proposed antenna was printed on the PET substrate by AgNPs ink and thermally treated with hot platen for 15min at 70°C. The curing was done immediately after the printing process since the AgNPs ink is easily oxidized, which results in poor radiation efficiency. After printing process, the SMA connector was attached to the printed antenna by using silver nanoparticles conductive epoxy paste and then antenna was cured at 50 °C for 2h. The resultant antenna is shown in **Figure 2.11** (a) and transparency as well as flexibility with low thickness of 0.04mm can be observed in **Figure 2.11** (b). Note that the fabricated antenna can be mounted on Telos-B as shown in inset of **Figure 2.11** (b).

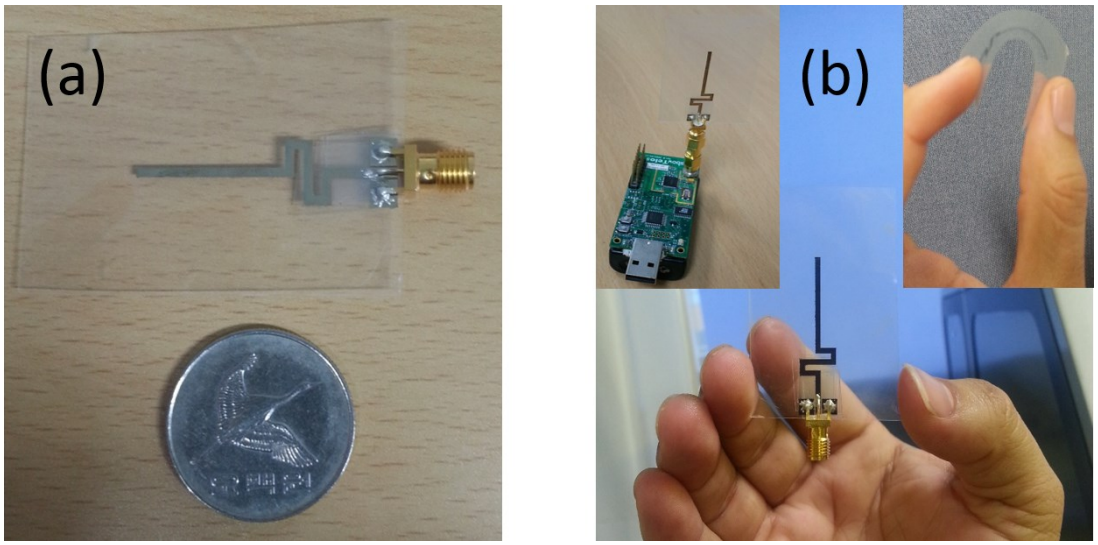

Figure 2.11. Proposed fabricated printed antenna on a PET substrate (b) Transparent and flexible PET (with 0.04mm thick) based printed antenna mounted on Telos-B (inset).

2.4 Characterization

Field Emission Scanning Electron Microscope (FESEM) image of the printed antenna pattern, as shown in **Figure 2.12**, which clearly shows that the gaps between silver nanoparticles are diminished due to high temperature and long curing time. The SEM image also assures formation of solid metal conductive printed track, which provides percolation channel flowing conduction electrons.

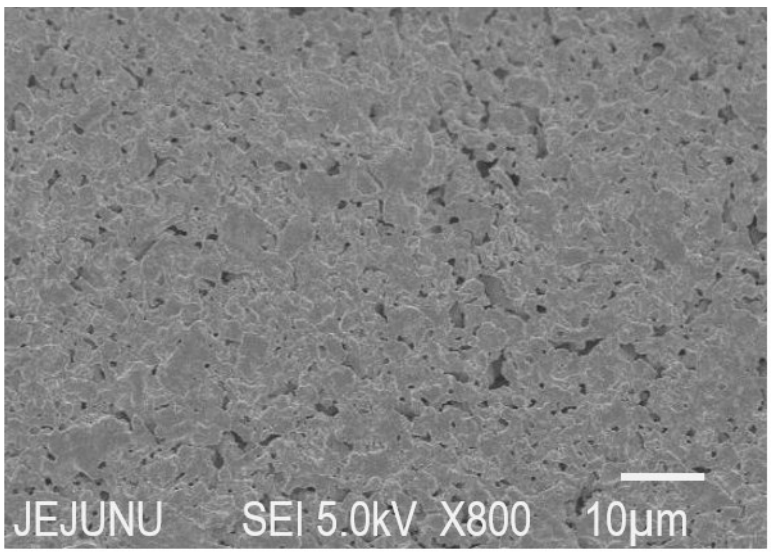

Figure 2.12. SEM Image of sliver nanoparticle ink layer after being cured at 50° for 2 h.

The electrical characteristics of antenna under test (AUT) are measured by two port calibrated HP VNA that is connected with 50Ω transmission line and 50Ω RF SMA connector as shown in **Figure 2.13** (a). The bendability and flexibility tests have been carried out by bending the AUT over radii of 2.5cm and 3.25cm. The received signal strength of AUT is measured by connecting the AUT with SA-7270 9KHz-2.7GHz LG spectrum analyzer.

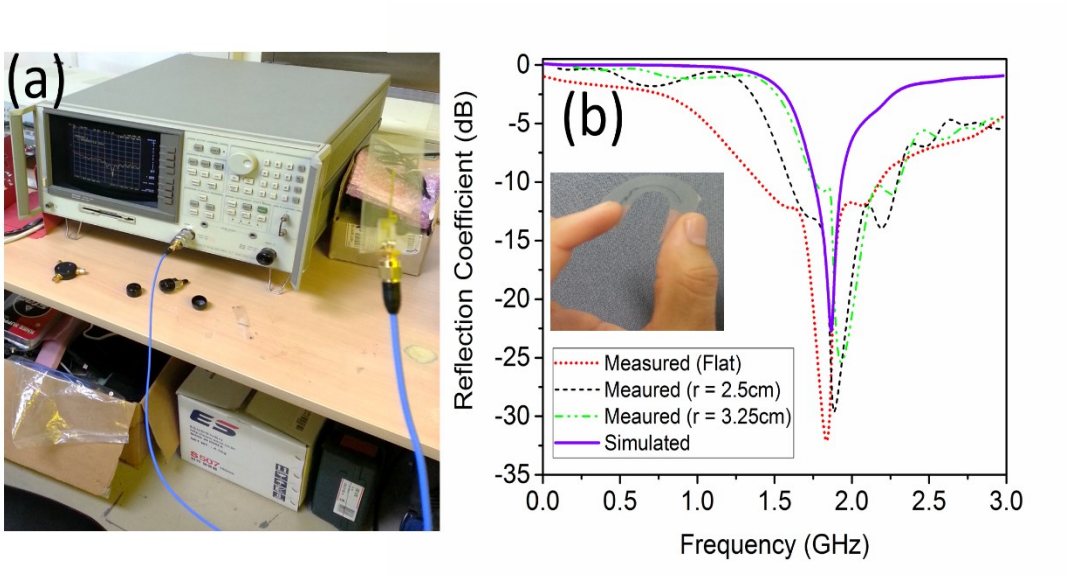

Figure 2.13. (a) Measured Reflection coefficient using HP vector network analyzer. (b) Measured (over different bending radii) and simulated reflection coefficient for the proposed printed antenna.

2.5 Results and Discussion

The proposed antenna performance was verified by simulation and measurement of resonance, gain, efficiency, reflection coefficient and received signal strength. The overall lumped circuit shown in **Figure 2.3** has inductance and capacitance of 0.7nH and 11 pF, respectively. The input reactance of the circuit model is shown in **Figure 2.14** , indicating resonance at the desired 1.8 GHz. The simulated radiations patterns of elevation (E-plane) and azimuth (H-plane) radiation patterns are shown in **Figure 2.15** (a) and (b), respectively. The simulated gain at 1.84 GHz resonant frequency is 2.72 dBi, which is reasonable as compared to other printed antennas [10-14], [30-31]. The simulated directivity at 1.84 GHz is 3.02 dBi and then total efficiency becomes -0.3 dB, which results in 93.33% efficiency. The front to back (F/B) ratio of 0.48 dB is observed in both elevation plane and azimuth planes, indicating that the proposed antenna is omnidirectional antenna. Also, we investigated the antenna performance

under extreme cases of the straight and complete meander type bending shapes. When the antenna completely bended in meander type shape, the resonance of the antenna was changed from 1.8GHz to 2.5GHz and gain was increased to 3.2dBi. However, in straight case the resonance was remained at 1.8GHz and 2.5dBi gain was observed. Similarly, the turn position and vertical length variations has been analyzed. The value of reflection coefficient was changed due to impedance mismatch however, the resonance and the gain of antenna were almost remained same in turn position analysis. While in vertical length variation resonance frequency as well as gain of the antenna changed (see section 2.2.3 for detail).

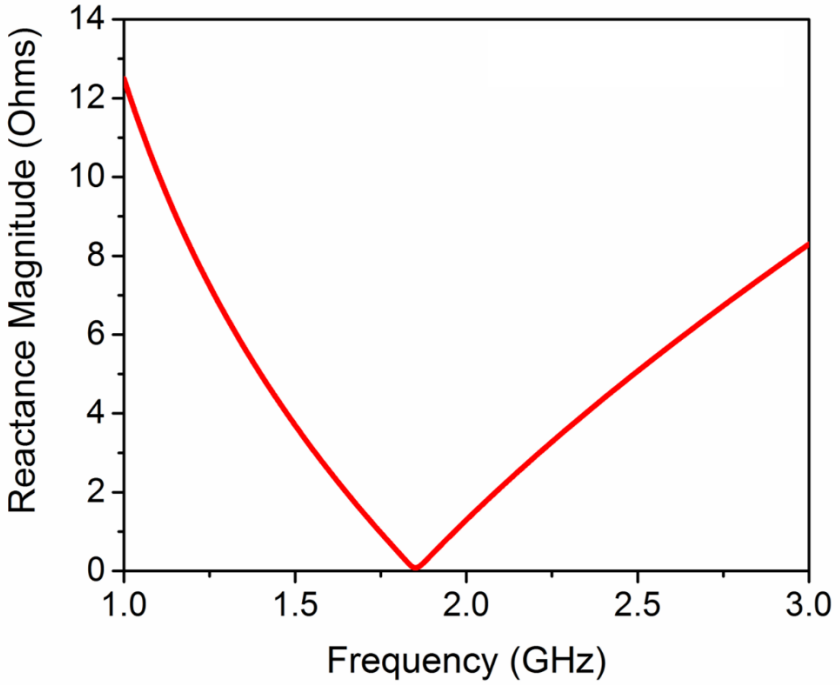

Figure 2.14. Input Reactance of the overall lumped model of the proposed antenna using NI multisim.

The electrical characteristics of antenna under test (AUT) are measured by two port calibrated HP VNA that is connected with 50Ω transmission line and 50 Ω RF SMA connector as shown in **Figure 2.13** (a). The measured and simulated reflection coefficients (S_{11}) are shown in **Figure 2.13** (b), in which we can observe that the measured resonant frequency is 1.84 GHz and the measured S_{11} is agreed with the simulation result. The measured -12 dB bandwidth is 280MHz (Δf_{Bw}= 15.56%) and the received signal strength measured by connecting the AUT with SA-7270 9KHz-2.7 GHz LG spectrum analyzer is -60.64 dBm at 1.84 GHz. This received signal

strength is consistent under background noise at 1.84 GHz as shown in **Figure 2.16**. Thus implies that the designed antenna can operate at real-world application using 1.84 GHz band.

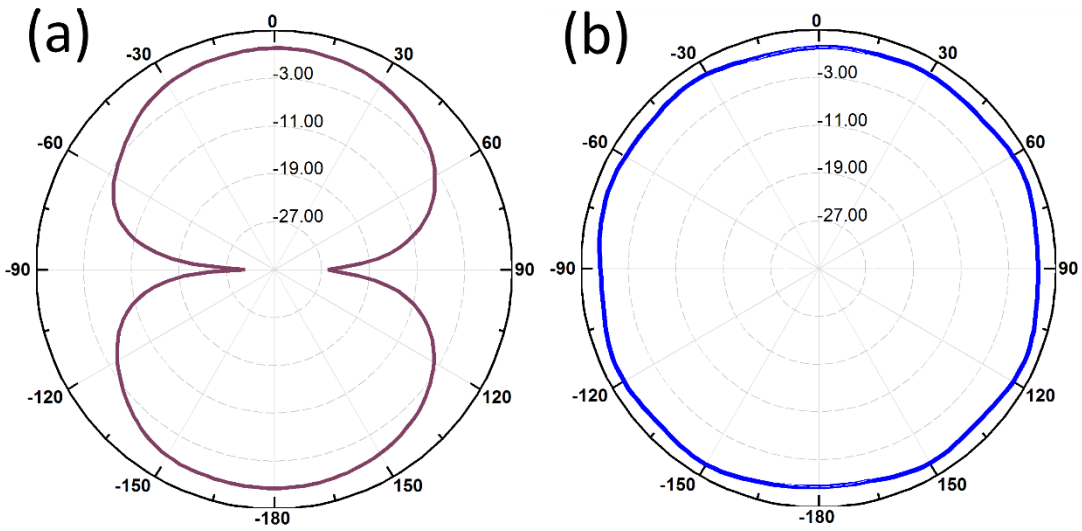

Figure 2.15. Radiation pattern of the proposed antenna (a) Azimuth (H-plane) radiation pattern (b) Elevation (E-plane) radiation pattern.

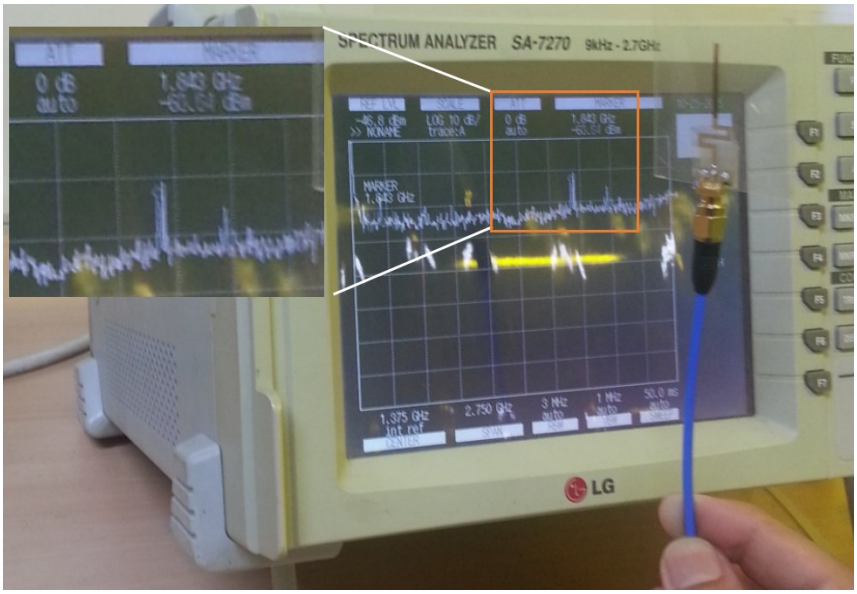

Figure 2.16. Received signal strength of proposed antenna.

The bendability and flexibility tests have been carried out to investigate the performance of the antenna under deformation. Bending of antenna causes change of resonance frequency as well as the reflection coefficient and impedance mismatch due

to change in its effective length. Reflection coefficient was measured by bending the AUT over radii of 2.5 cm and 3.25 cm. Consequently, the reflection coefficient decreases and resonance frequency shifted from 30-60 MHz to higher frequency under convex bending as shown in **Figure 2.13**. Even the reflection coefficient degraded with bending, AUT performed well since the reflection coefficient was still less than -10 dB.

After restoring to its original position, no permanent deformation and deterioration has been observed. The performance was not deteriorated during bending experiments, carried out more than hundred times.

Table 2.4. Comparison of different flexible antenna with the proposed antenna.

Characteristics	Proposed PET based antenna	Kapton based antenna [10]	Textile based antenna [11]	Paper based antenna [12]	Fluidic based antenna [13]	Flexible Bow-tie antenna [14]
Size mm	**9.49 x 43.35**	**26.5 x 25**	**180 x 150**	**46 x 35**	**54 x 10**	**39 x 25**
Thickness mm	0.04	0.05	4	0.25	1	0.13
Band/f	Single/1.84 GHz	Single/2.4GHz	Dual/2.2GHz, 3GHz	Single/2.4GHz	Single 1.85GHz	Single/7.6GHz
Substrate	PET ϵ_r=2.8	Kapton ϵ_r=3.4	Felt Fabric ϵ_r= 1.5	Paper ϵ_r= 3.4	PDMS ϵ_r=2.67	PEN Film ϵ_r=3.2
Dielectric loss	Low loss tanδ =0.003	Low loss tanδ =0.002	High loss Low loss tanδ =0.02	Low loss tanδ =0.065	Low loss tanδ =0.37	Low loss tanδ =0.015
Tensile Strength	High (266 MPA)	High (165 MPA)	Low (2.7 MPA)	Low (30 MPA)	Low (3.9 MPA)	High (74 MPA)
Flexural Strength	High (20000 p.s.i)	High (50000p.s.i)	High (8900 p.s.i)	High (7200 p.s.i)	High (650 p.s.i)	High (13564 p.s.i)
Deformability	Low	Low	High	High	High	Low
Thermal stability	High	High	Low	Low	Low	High
Fabrication Complexity	Simple/ Printable	Printable	Complex/ non printable	Printable	Complex/ non printable	Printable
Gain	2.72dBi	1.65dBi	Not specified	1.2dBi	Not specified	2.3dBi
Bandwidth	190.5MHz	430MHz	100MHz @-6dB	550MHz	400MHz	1.7GHz

The proposed antenna is comparatively analyzed, as shown in **Table 2.4**, with different flexible antennas presented in [10-14]. The antenna is analyzed on the basis of electrical and mechanical properties. The main focus of this comparative analysis is on compactness and robustness. Flexibility, deformability, thermal stability and tensile strength are the major mechanically properties considered to investigate the robustness of the proposed antenna. Fabrication process and its complexity are also included in this analysis. **Table 2.4** shows that the proposed antenna design is relatively compact, fully flexible, robust and small in loss factor (tanδ). The gain of the presented antenna is high as compared to other printed antennas, whereas the bandwidth is relatively small. The simple fabrication process on a low-cost PET substrate allows industrial roll to roll (RoR) production and also, further weight reduction for antenna integration with RF IC.

2.6 Summary

We proposed a novel ink-jet printed antenna on 40 micron thick, flexible and transparent PET substrate for 1.8 GHz band applications. The antenna was designed and simulated via HFSS and was verified through NI Multisim simulation using equivalent circuit model. The proposed antenna has achieved gain and efficiency of 2.72 dBi and 93.33% respectively. The antenna was realized with commercialized DMP-3000 by depositing silver nanoparticles ink as radiating element and ground on the UV treated PET substrate. The fabricated antenna has shown reflection coefficient of -32.2 dB at 1.84 GHz band which agrees with simulation result. These results indicates that the proposed antenna can be used for transparent and flexible wearable electronic devices using 1.8 GHz band.

Chapter-3 Flexible Dual-band Antenna

3.1 Why flexible dual-band antenna?

3.1.1 Introduction

Nowadays, Wi-Fi communication is popular since it is the most common standard for wireless communication operating in free industrial, scientific and medical (ISM) band. The standard Wi-Fi protocols of IEEE 802.11b and 802.11g use 2.45 GHz, while the IEEE802.11ah utilizes 900 MHz [49-50]. The electronic devices for all Wi-Fi protocols need integration of low-profile and low-cost dual band antenna [30]. Conventional manufacturing technology based on lithography can produce device with high accuracy. However, this fabrication process is quite complicated, time consuming and requires precise control of temperature and pressure. Other drawbacks are throughput limitations, lack of batch processing and use of rigid substrates and corrosive chemicals [3], [33], [36], [38-39].

Recently, printed electronics technology has emerged as a promising technology and widely investigated as the technology is low-cost, handy, and can operate with immediate and single-step process. The printed electronics has been used for mass production of low-cost and flexible electronic devices such as RFID antennas, OLEDs, OTFTs and organic memory [3], [33-34], [36].

Many researchers have utilized the printed electronics for antenna design and used gold and copper to achieve good radiations [36]. However, gold and copper having high curing temperature, cannot easily be printed on flexible polyamide substrate [39-40]. On the other hand, common nanoparticle ink of silver (Ag) becomes suitable for fabrication of low-cost flexible antennas since its melting temperature is low and compatible with flexible polyamide film and paper substrates.

The use of low-cost flexible substrate with low loss factor such as paper, Kapton and polyimide film have been reported [27], [30-33]. Common paper substrate has high tangent loss factor of 0.065 yet it cannot withstand hard environmental conditions. Kapton and polyamide substrates provide cost effective solution for Roll-to-Roll (R2R) mass production and also they are foldable, bendable and transparent [27], [30-

33]. Polyethylene terephthalate (PET) is thin, flexible, foldable and transparent. The glass transition temperature of PET is in the range of 80~100 °C so that PET is mostly used for synthetic fiber and liquid or food container [13]. Printed electronic devices and R2R processing using PET have been reported [3],[33], [34],[36], [38].

The surface roughness of PET is lower than paper and Kapton so that PET has small reflection loss [38]. The tangent loss of PET is as low as 0.003 at 1 GHz [53] so that it is adequate for high frequency applications. Antenna designs on PET substrate have been demonstrated and cost-effective and inkjet-printable antennas on PET have been developed [38-40], [54-55]. Flexible antenna on PET for single 1.8 GHz band has been reported [56]. This antenna was designed for such small device as TelosB and yet antenna gain was as low as 2.7 dBi. A dual band antenna based on Yagi log-periodic dipole array (LPDA) for wireless communication was reported [57]. The LPDA antenna was fabricated on 1 mm thick PET and designed for both WLAN-UHF band (2.4~2.5 GHz) and WLAN-SHF (5.2~5.8 GHz) band. The gain of the LPDA printed on 111.98 mm × 55 mm substrate, were reported as 5.5 dB at WLAN-UHF band and 6 to 7 dB at WLAN-SHF band.

In this paper, we propose a compact patch antenna, which has high gain and operates on dual Wi-Fi band of 900 MHz and 2.4 GHz. The proposed antenna is printed on 50-micron thickness PET substrate so that it is fully transparent and suitable for wearable devices. For antenna design, we use the HFSS and for antenna fabrication, we use commercial DMP-3000 printer by depositing AgNPs on PET substrate. Through simulations and experiments, we proved that the proposed antenna has high gain at dual bands and that is robust to severe bending and folding of antenna.

3.2 Antenna Design

The antenna structure is comprised of Z-shaped radiating monopole element fed by co-planar waveguide (CPW). The CPW feeding technique not using via-hole connection or shorting pins, has key advantage that radiating body and ground plane can be printed on the same side of substrate. This significantly reduces production cost since printing process becomes fast, simple and roll-to-roll production is possible. Furthermore, it has low radiation loss, improved impedance matching and larger bandwidth as well. The size of the antenna is minimized by adopting ring (Z) based winding, which provides longer path for current flow and minimizes significant effect

on radiation pattern. We obtained optimum separation between the radiating arms (W_s) as 9mm, which matches with 50 ohms input and reduces coupling effect between arms as well. The smaller separation than 9mm increases coupling effect and hence, degrades the antenna performance of impedance matching. The Z-shape monopole antenna fed by 3.5 mm wide CPW is printed on same side of the substrate. Contrary to the dipole antenna, the monopole antenna uses its ground as radiating surface and prevents the antenna from external electronic circuit effects as current leakage and electrical surge etc.

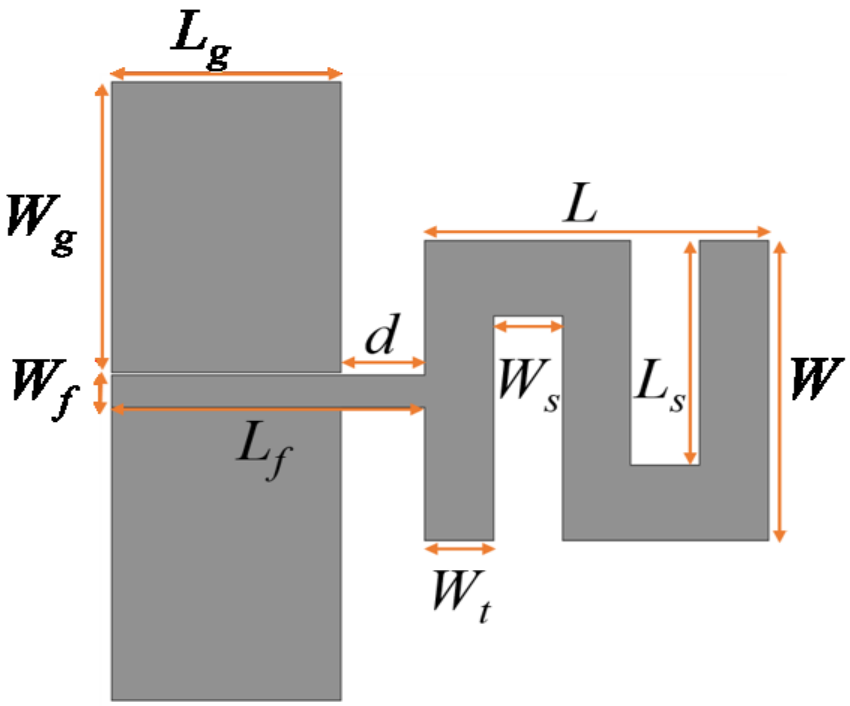

Figure 3.1. Geometry of antenna

To achieve dual band characteristics, we adjust length Ls and width Ws of the rectangular slots inside the L × W rectangular monopole. The Ls is adjusted for radiation at specific band and the number of transition is adjusted for bandwidth and gain requirement of the band. Note the antenna has two current flows i.e. longer path and shorter path. The longer meander type path has total length of 151.61mm (Lf + Wf/2 + W/2 + 2Ws + 2W), which is approximately equal to one-half wavelength of 900MHz. Similarly, the shorter path has total length of 61.61mm (Lf + Wf/2 + W/2), which is approximately equal to one-half wavelength of 2.4GHz. Consequently, the proposed antenna structure produces dual resonant modes. Increasing the size of the

ground slightly increases directivity of antenna with the expense of size increment. The distant (*d*) between the radiating element and the ground give primary influence on both radiation pattern and antenna impedance. Radiation of antenna highly depends on the length of first transition so that it should be separate enough to allow good wave conformation into free space.

Using these design considerations, we obtain the size of monopole antenna as 45mm × 36 mm and the size of two rectangular slots as 27 mm × 9 mm (symmetric on both edges), which are inserted into the monopole for both impedance matching and radiation at dual bands. The resultant Z-shape antenna is as shown in **Figure 3.1** and the parameters are given in Table 3.1. To print the antenna, we deposit the AgNPs on 86.9 mm × 54.7 mm PET substrate, which is transparent, flexible, 0.05 mm thick, dielectric constant of 2.8 and loss tangent of 0.003 at 1GHz frequency [53]. Note that the proposed design has L × W rectangular structure containing two Ls × Ws symmetric slots inside the structure, which has dual band characteristics differentiating the single band antenna [56] having straight line and meander geometry in the middle. In addition, the proposed dual band antenna has much higher gain than the antenna in [56].

Table 3.1. Design parameters of the proposed antenna.

Parameter	Dimension (mm)	Parameter	Dimension (mm)
L	45	d	11.86
W	36	W_s	9
L_g	30	L_s	27
W_g	25.02	L_f	41.86
W_t	9	W_f	3.5

3.3 Experiment

We have utilized Ansys HFSS to evaluate the performance of the proposed antenna. By sweeping frequency from 0.1 MHz to 6GHz, we obtained reflection coefficients with two dip points at 900MHz and 2.4GHz bands. Similarly, we obtained gain, directivity and radiation patterns corresponding to 900MHz and 2.4GHz. For printing, the verified design was exported into ACE3000 software along with all geometrical information. The printing setup is as shown in **Figure 2.10**. Before initializing printing process, all the printing parameters were adjusted by printing software of Dimatix Drop Manager (DDM).

3.3.1 Material

The AgNPs ink (3ml) purchased from Sigma Aldrich South Korea, was filled into the cartridge of 16 nozzles with diameter of 42µm and distance of 508µm. To print the antenna, we select 10pl of single drop and use PET film for substrate. However, initial PET surface is usually rough with scratches and contaminations with some organic materials, so that we cleaned it with ethanol baths at ambient condition, rinsed it with water and dried it at 100°C for 2 minutes before printing.

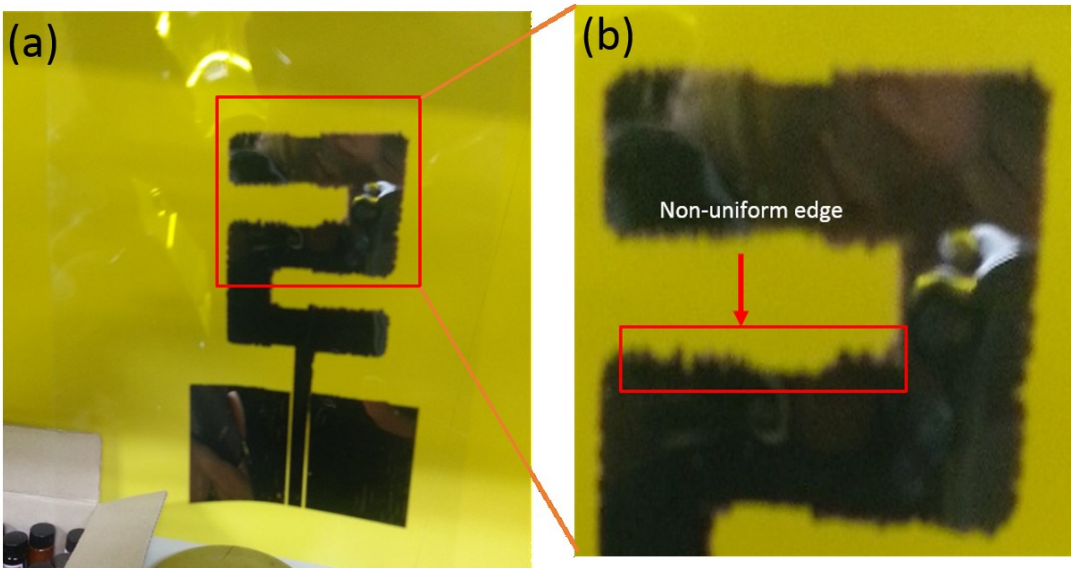

Figure 3.2. (a) Antenna pattern obtained with 5 min UV treatment. (b) Partially magnified pattern showing non-uniform edge.

3.3.2 Fabrication Process

we obtained initial antenna made of randomly spread AgNPs ink over the PET surface and of non-uniform edge, as shown in **Figure 3.2** (a) and (b). To remove these problems, we treated the PET as 4 minutes UV treatment. The UV treated PET was placed onto 50 °C heated platen in inkjet printer. Yet random spreading problems occurred again. Throughout experiments, finally we obtained that 30 seconds of UV treatment and temperature of 25° C produce optimum result. The resulting printed antenna was thermal treated with hot plate for 5 minutes at 40 ° C. For feeding signal, we attached 3.5mm subminiature version A (SMA) to the CPW feed line by using sliver epoxy paste. The consequent antenna is as shown in **Figure 3.3** (a) and (b).

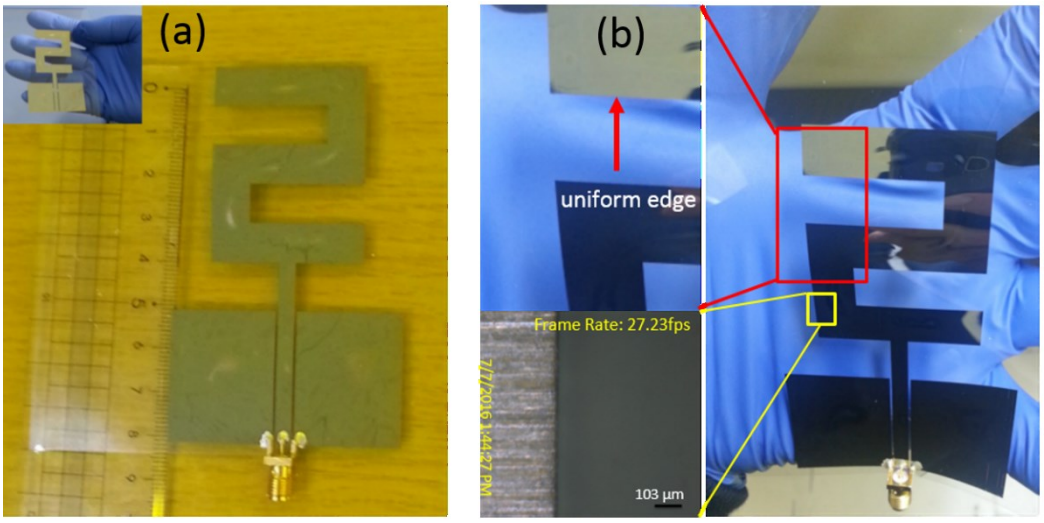

Figure 3.3. (a) Fabricated antenna with ruler and the transparent antenna pattern shown in inset. (b) Partially magnified pattern showing uniform edge with 30 sec UV treatment.

3.3.3 Surface Morphological Characterization

In order to characterize surface morphology of the proposed antenna, we used the NV-2000(Universal), non-contact 3D surface profiler of nanoscale precision. By using phase shifting interferometry (PSI) mode in the profiler, we obtained 3D profile of silver antenna pattern over PET substrate, as shown in **Figure 3.4** (a). It can been seen that the silver pattern is uniform deposited with thickness of 480nm. By using the Jeol JSM-7600F, we subsequently obtained scanning electron microscopy (SEM) image of silver antenna pattern with 10µm scale, as shown in **Figure 3.4** (b). We can observe uniformly deposited silver layer over the PET surface.

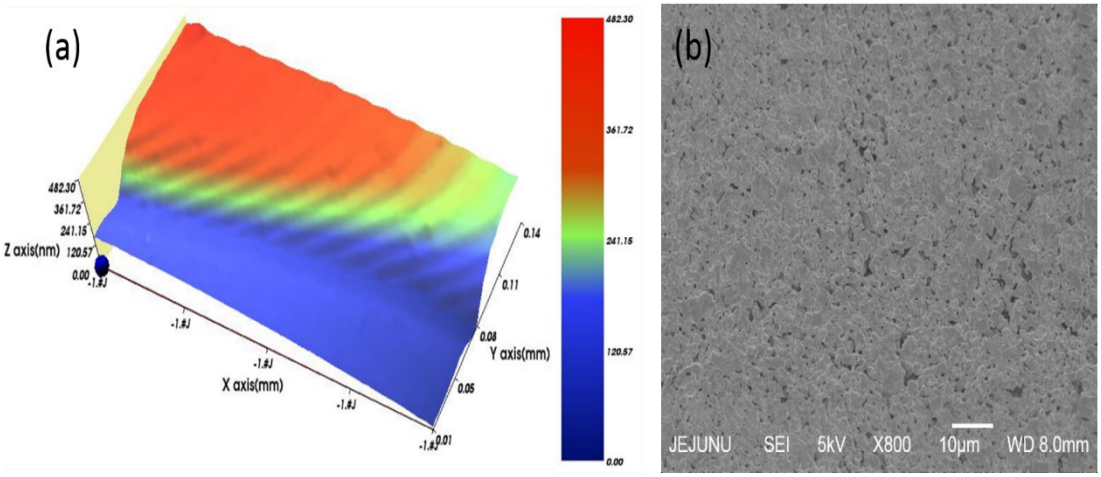

Figure 3.4. (a) 3D surface profile of silver pattern deposited with 480nm thickness. (b) SEM image of silver nanoparticle ink pattern obtained with 10µm scale.

3.3.4 Electrical Characterization

To characterize the printed antenna, we use calibrated HP VNA connected with 50Ω transmission line and 50Ω RF SMA connector as shown in **Figure 3.7** (a). We measured the reflection coefficient by sweeping the frequency from 30 kHz to 3GHz.

3.4 Results and Discussion

The simulated azimuth (H-plane) and elevation (E-plane) radiation patterns are as shown in **Figure 3.5** (a-d). The obtained antenna gains are 16.74dBi at 900MHz and 16.24dBi at 2.4GHz and directivities of 16.76dBi at 900MHz and 16.73dBi at 2.4GHz, which are superior to the LPDA [57]. The obtained radiation efficiency is -0.02dB corresponding to 99.63% efficiency in lower 900MHz band. In terms of 3D radiation patterns shown in **Figure 3.5** (e-f), the printed antenna is omnidirectional at 900MHz but slight directional at 2.4GHz. We also present surface current distributions of feeding line, radiating patch and ground in **Figure 3.6**.

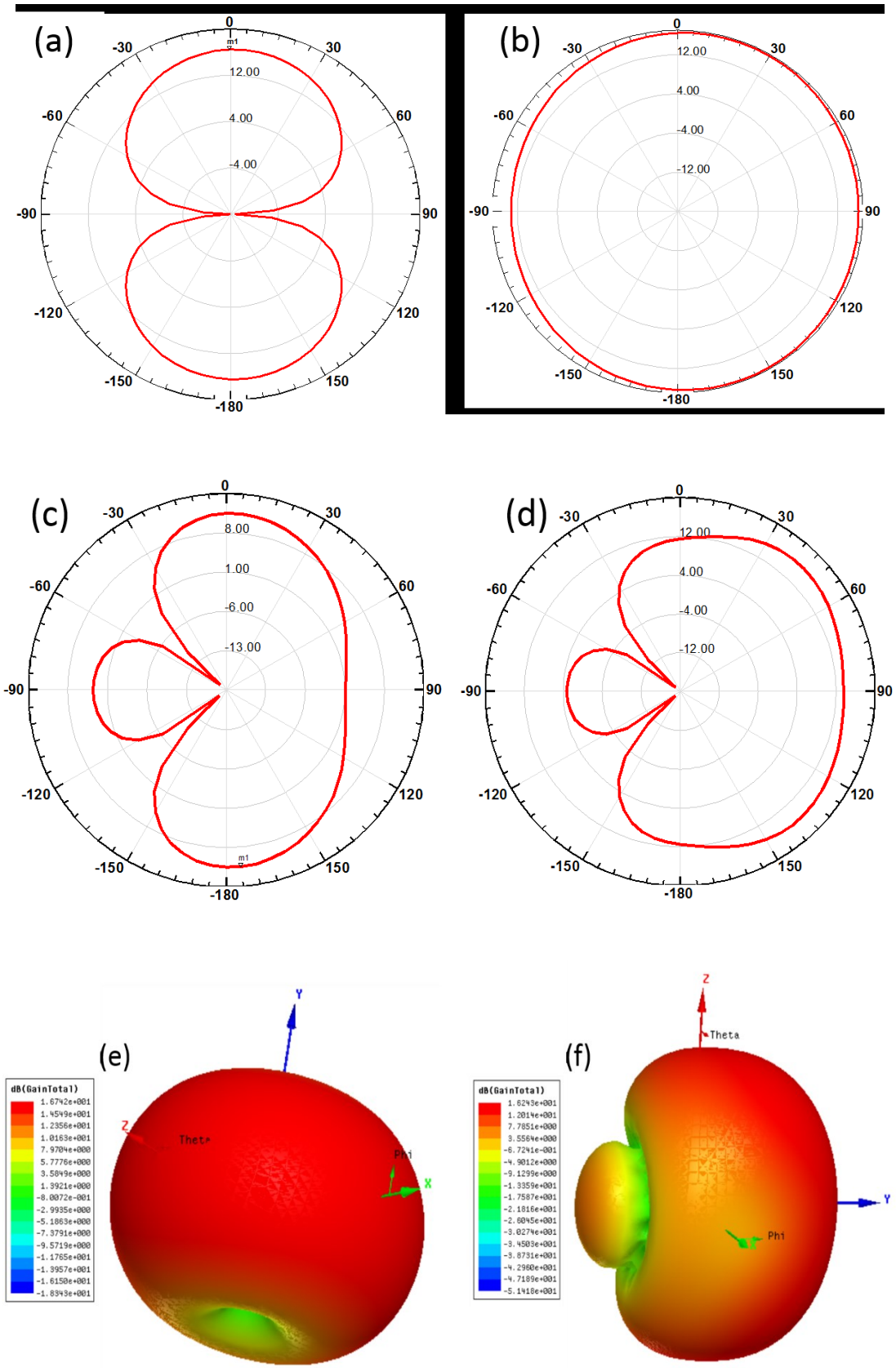

Figure 3.5. Radiation patterns of the proposed antenna (a) Azimuth pattern at 900MHz showing 16.74dBi gain. (b) Elevation radiation pattern at 900MHz. (c) Azimuth pattern at 2.4GHz showing 16.24dBi gain. (d) Elevation pattern at 2.4GHz. (e) 3D pattern at 900MHz. (f) 3D pattern at 2.4GHz.

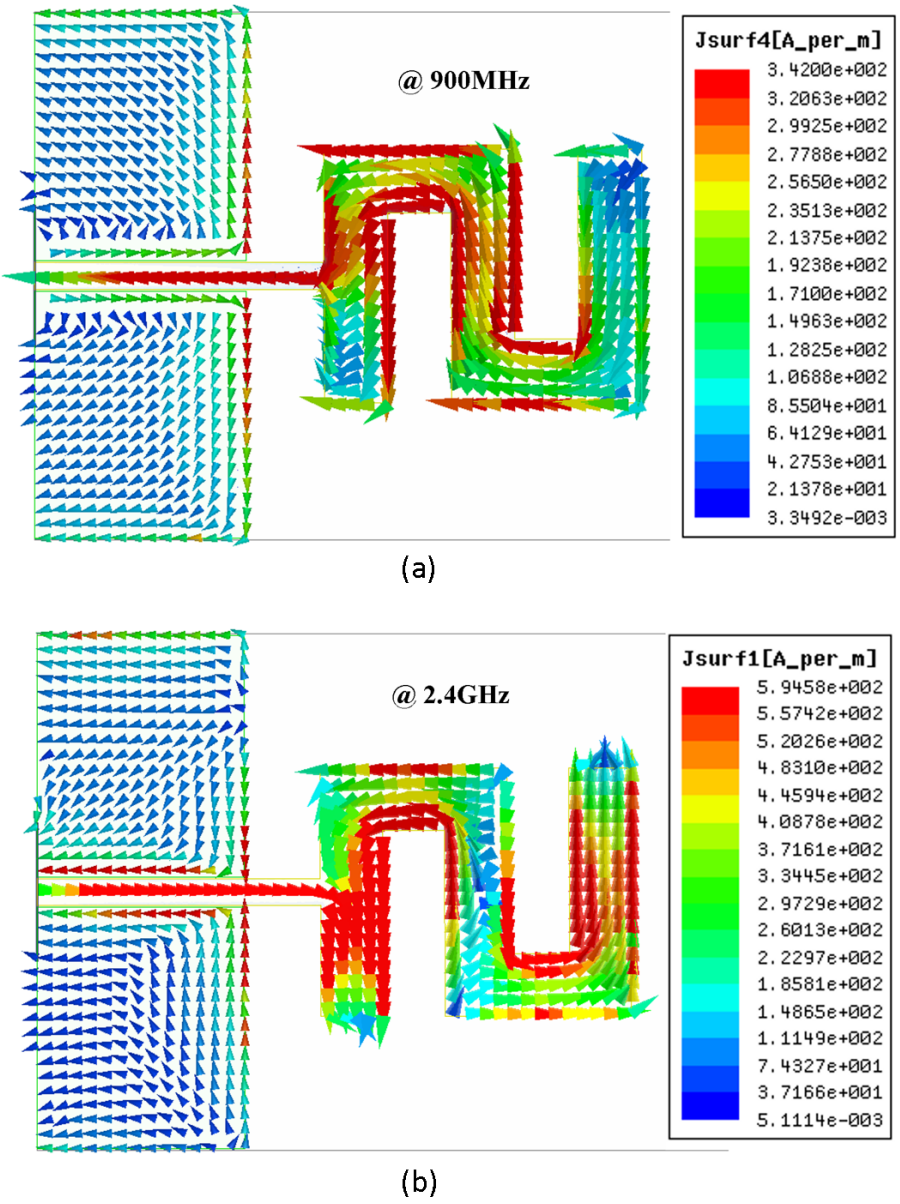

Figure 3.6. Surface Current analysis of the antenna (a) at 900MHz and (b) 2.4GHz.

We can observe high current density along the longer path in **Figure 3.6** (a), which has low impedance and maximum radiation at 900MHz. Similarly, **Figure 3.6** (b) shows high surface current density along the shorter path having low impedance and maximum radiation at 2.4GHz. These results clearly show that the proposed antenna radiates at both 900MHz and 2.4GHz, even though current density at the end is relatively low due to high impedance at the ends.

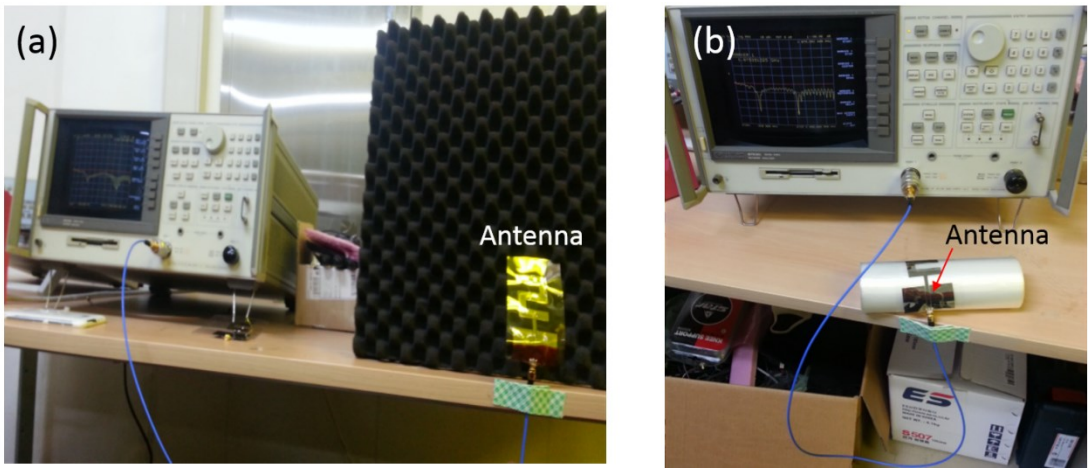

Figure 3.7. (a) Measurement setup for reflection coefficient. (b) Setup for flexibility test with cylinder of 5.86cm radius.

For flexibility and bendability test, we placed the AUT on cylinder of radius 5.86cm as shown in **Figure 3.7** (b). Consequently, we observed resonant frequency shift from 0.9GHz to 0.75GHz and 2.4GHz to 2.2GHz, and S_{11} changes -30.9dB at 0.75GHz and -34dB at 2.2GHz, as shown in **Figure 3.8**.

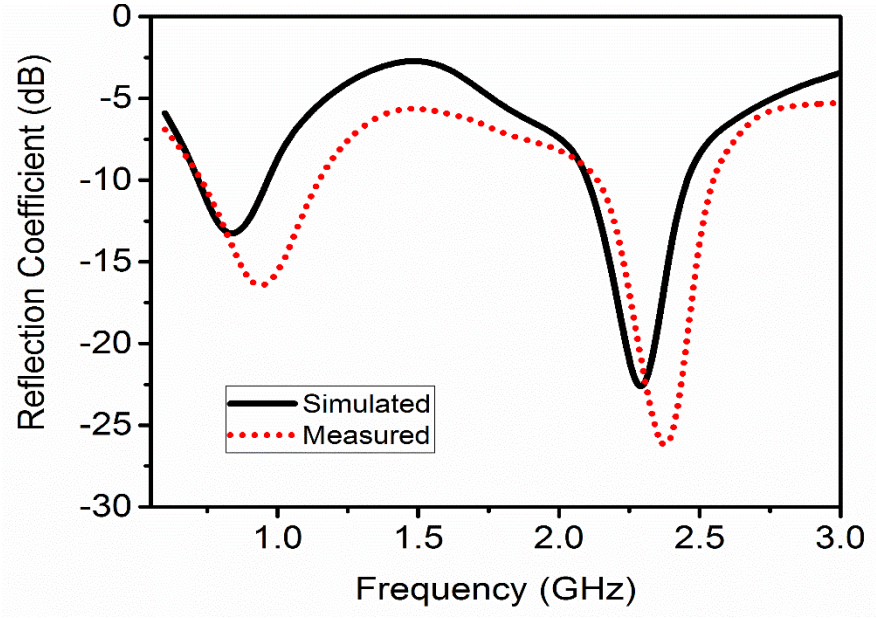

Figure 3.8. Measured and simulated reflection coefficients of the proposed dual band antenna.

Under complete folding condition, as shown in inset of **Figure 3.9**, we obtained reflection coefficient of -11.1dB at 0.75GHz and -23dB at 2.3GHz. Despite degradation of reflection coefficient, note that the AUT can operate properly as S_{11} is

less than -10dB at 0.75GHz and 2.3GHz. Consequently, we can conclude that the proposed dual band antenna is robust to deformation so that remains fully functional.

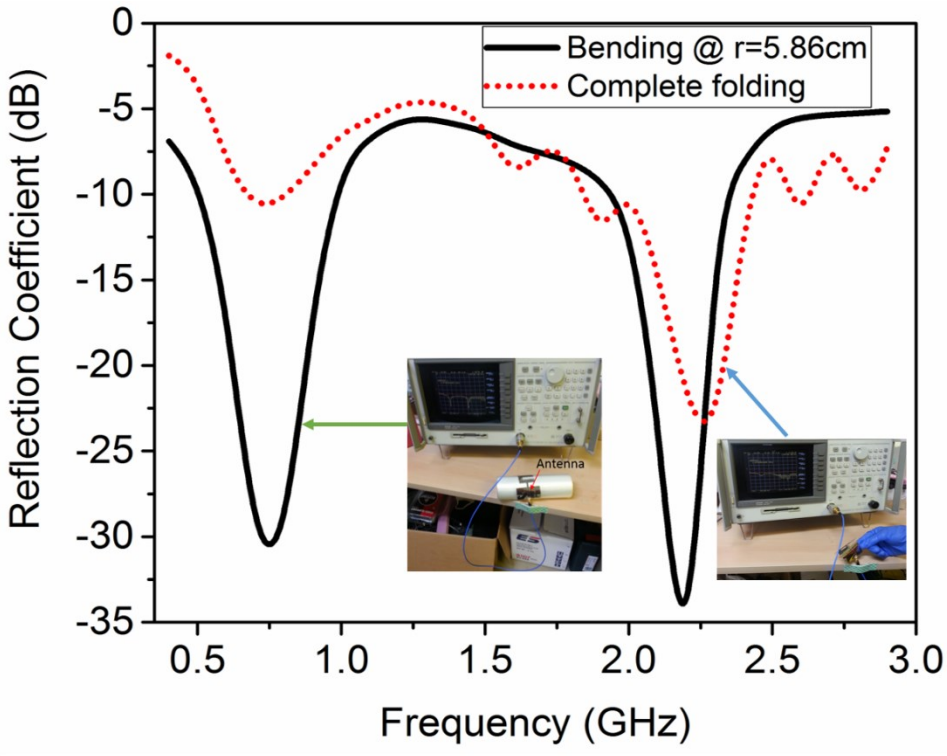

Figure 3.9. Reflection coefficients measured with 5.86cm radius bending and with complete folding.

3.5 Summary

We have proposed a high gain antenna for flexible electronic devices working on dual Wi-Fi bands. For antenna design, we used the Ansys HFSS and we used the DMP-3000 depositing AgNPs on 50-micron thin PET substrate for antenna fabrication. The fabricated dual band antenna has significant S_{11} dips of -16.45dB at 900MHz and -26dB at 2.4GHz and has high gains of 16.74dBi at 900MHz and 16.24dBi at 2.4GHz. The -10dB fractional bandwidths of the proposed antenna are 23.33% at 900MHz and 11.66% at 2.4GHz bands. Throughout folding and bending test, we proved that the proposed antenna is robust to external deformation. These results assure that the proposed low-cost, high gain and dual band antenna is well suited for wearable devices requiring dual Wi-Fi band.

Chapter-4 Transparent Antenna

4.1 Transparent Antennas

In the last decade, numerous antenna designs have been demonstrated for Wi-Fi band [27]. Similarly, the unlicensed ISM band communication attained much interest due to free communication over 2.4 GHz. The Prior ISM band microstrip antennas were mostly fabricated on rigid surface of FR-4 board, which are not suitable for wearable electronics. Printed technology allows us to fabricate wearable and low cost electronic devices and systems because it requires low processing temperature [58]. Recently, flexible printed antennas were reported for the Wi-Fi band [27-31]. Since wearable electronic devices need wireless connectivity, a flexible printed antenna is required. Previously, flexible antennas have been demonstrated on various substrates including paper, electro textile, kapton polyimide film, and polymer [27], [28-31]. All of these designs used conducting films like copper and silver with the opaque substrates while paper based substrates are not enough robust to with stand in hard ambient condition and also have a high loss tangent value (around 0.07 at 2.45 GHz) [27], [31].

In [32], authors has demonstrated an antenna design with silver nanowires (AgNWs) on the PDMS substrate. However, the presented design is not transparent and their peak directivity is low. To get transparency, the previous reported antennas used a rigid glass as a substrate. Recently, to fabricate transparent antennas, transparent indium tin oxide (ITO) and fluorine doped tin oxide (FTO) conductive films are utilized [59-60]. These films allow transmission of electric currents while provide good optical transparency [61]. However, the reported antennas using ITO and FTO are not studied for ISM band as well as for transparent substrates. In addition, the performance of these antennas is not investigated under deformation such as bendability, tensile strain, and reversibility. In our proposed antenna, we utilize ITO instead of FTO as the optical transparency and electrical conductivity of ITO is better than FTO [62].

In this paper, we propose a transparent, flexible, and bendable inset microstrip patch antenna for Wi-Fi band, which is fabricated by depositing the ITO for both patch and ground plane on a PDMS substrate through commercialized Fujifilm inkjet dimatix material printer (DMP-3000). The proposed antenna for ISM band is designed and

simulated in Ansys HFSS software, which is characterized for mechanical, electrical, and optical characteristics. The measured dip of the reflection coefficient (S_{11}) and the theoretical gain of the antenna on the flat position are -25.9 dB and 5.75 dBi, respectively. At 1.5 mm thickness, the bendability of the proposed antenna down to 10 cm is tested. The reversible deformation time and the transparency of the antenna are characterized at its thickness of 1 mm, 1.5 mm, and 2 mm.

4.2 Microstrip Design

To get transparent and bendable characteristics, the proposed antenna consists of a thin ITO based patch and ground plane on the dielectric substrate of PDMS as shown in Figure 4.1 (b), and the logo can be seen through the antenna which indicates its transparency. The electrical conductivity of 400 nm thick transparent ITO film is 2.88×10^5 S/m while the copper with the same thickness has electrical conductivity of 5×10^6 S/m, which is a little bit high as compared to transparent ITO based film [63-64]. The electrical conductivity of the ITO film increases with increasing the thickness but its optical transparency decreases [61]. The relative permittivity of the PDMS has ranging from 2.67 to 2.80 while loss tangent from 0.01 to 0.05 over frequency range of 1 to 5 GHz [32]. In order to obtain 2.4 GHz resonant frequency, the parameters of the rectangular patch, as shown in Figure 4.1 (a), are given in **Table 4.1**. In Figure 4.1 (a), W_p and L_p are the width and length of the patch antenna, respectively. The value of W_p and L_p are calculated by using equations (1) and (2) respectively [43].

$$W_p = \frac{c_0}{2 f_r} \sqrt{\frac{2}{\varepsilon_r + 1}} \tag{1}$$

$$L_p = \frac{c_0}{2 f_r \sqrt{\varepsilon_{reff}}} - 2\Delta L_p \tag{2}$$

where f_r represents the resonant frequency which is 2.4GHz for the given design. The ε_r and c_0 describes the relative permittivity of the substrate and light velocity in free space respectively. The effective permittivity of the substrate is given by equation (3).

$$\varepsilon_{reff} = \frac{\varepsilon_r + 1}{2} + \frac{\varepsilon_r - 1}{2} \left[1 + 12 \frac{h}{W_p}\right]^{-\frac{1}{2}} \text{ for } \frac{W_p}{h} > 1 \tag{3}$$

There is fringing effect at the edges of the radiating patch due to this effect the physical length (L_p) of the radiating patch decreases from the actual length by a ΔL_p length which is given by equation (4).

$$\Delta L_p = 0.412h\frac{(\varepsilon_{reff} + 0.3)\left(\frac{W_p}{h} + 0.264\right)}{(\varepsilon_{reff} - 0.258)\left(\frac{W_p}{h} + 0.8\right)} \tag{4}$$

where the thickness of the antenna is represented by h. The width and length of the inset feed line in the rectangular patch are shown by W_f and L_f respectively. The notch width is represented by g which is symmetric along the width of the patch. The inset depth is given by d which represents distance from the radiation edge. The substrate length and width are denoted by L_s and W_s, respectively. Our design parameters as given in **Table 4.1** are obtained by simple calculation utilizing equations 1 and 2.

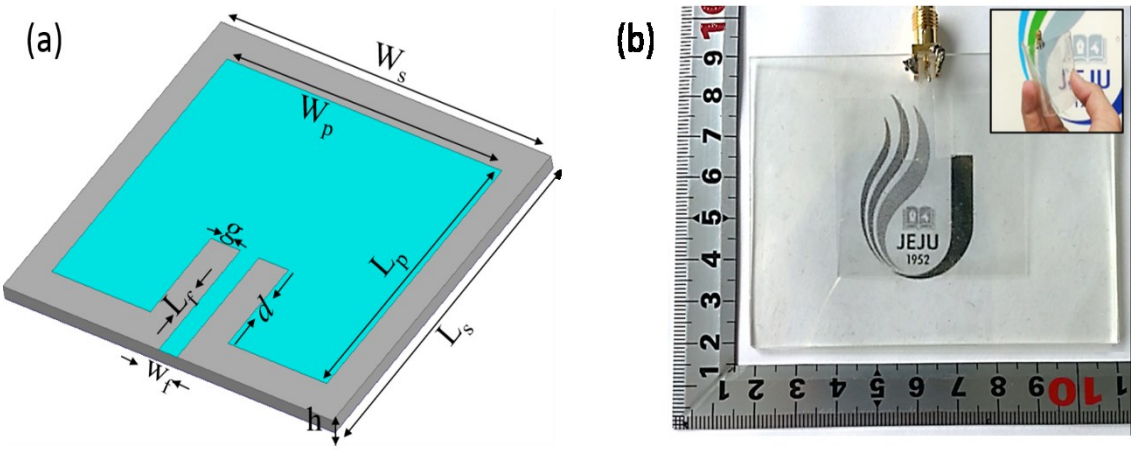

Figure 4.1. The proposed inset microstrip patch antenna based on PDMS/ITO. (a) Antenna geometry for design and simulation. (b) Fabricated antenna flat and its flexible view (inset).

Table 4.1. Simulation and design parameter of the proposed antenna.

Parameter	Dimension (mm)	Parameter	Dimension (mm)
L_p	36.8	L_f	20.6
W_p	45	W_f	3.9
L_s	80	d	12.77
W_s	100	g	2.7

4.3 Material and Methods

4.3.1 Material

To fabricate the proposed antenna, ITO ink was purchased from sigma Aldrich South Korea and the PDMS substrate was prepared as: (1) the base and the curing agent of PDMS material (Dow Corning's Sylgard 184) were mixed with 10:1, second, (2) the PDMS solution was casted in a tray with designed thickness, thereafter it was cured at 80 °C for 30 min. The PDMS substrate was cut in 8×10 mm^2 size and then treated UV ozone for 10 min to improve ink adhesion. The ink was filled into the cartridge of DMP-3000 inkjet printer containing 16 nozzles and the HFSS design file was exported to Dimatix Drop Manager (DDM).

4.3.2 Fabrication

The PDMS substrate was placed on the hot platen of DMP-3000 and printing parameters were adjusted by using DDM. Using ITO ink, a patch was deposited through DMP-3000 on the manufactured PDMS substrate, and it was cured at 160 °C for 1 hr. After then, a ground plane was also deposited with same printing parameters as described in **Table 4.1** and cured again for 1hr. The material and fabrication process is shown in Figure 4.2. The fabricated antenna and its flexible view (inset) is shown in Figure 4.1 (b)

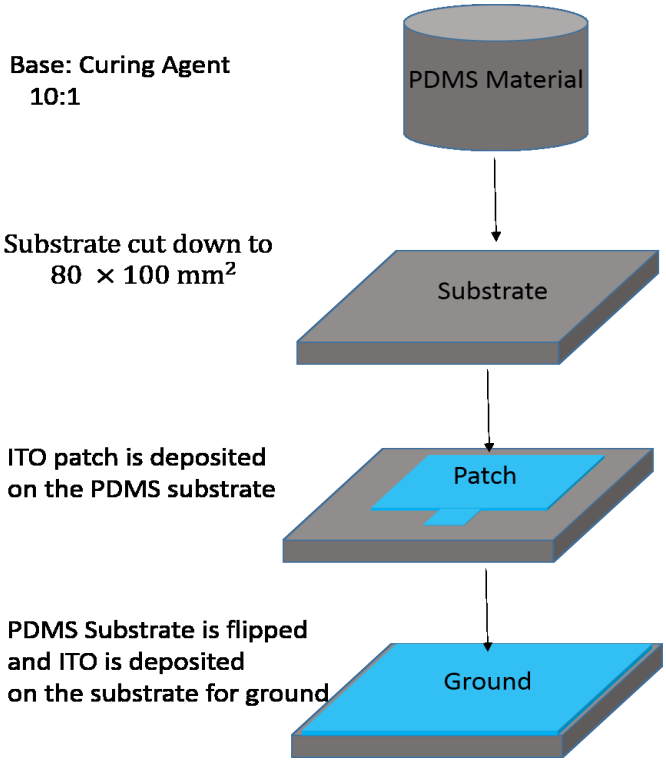

Figure 4.2. Material and fabrication process.

4.4 Characterization

4.4.1 Electrical Characterization

The HP 8753D vector network analyzer (VNA) 30 KHz – 3 GHz was utilized to measure the reflection coefficient of the fabricated antenna. First, the VNA was calibrated by using Agilent calibration kit. To ensure the correct measurement, SOL (Short, Open, Load) calibration has been carried out before measurement. After that, the AUT was connected with VNA through coaxial cable (50 Ω) and Sub Miniature version A (SMA) RF connectors (3.5 mm) at ambient conditions.

4.4.2 Optical Characterization

To optical characterize the printed antenna, the optically transparency experiment was verified by using Shimadzu – UV/VIS/NIR-3150 spectrophotometer. We loaded the AUT in the sample holder and placed it inside the spectrophotometer. Afterwards, we passed the light through the AUT and collected the data. **Figure 4.5** shows the optically

transmission of the light from the proposed ITO/PDMS material antenna over different thickness.

4.4.3 Mechanical Characterization

The AUT was characterized against mechanical deformation by flexing the antenna with hand and measuring reflection coefficient at each mechanical stress. The antenna was bent from flat position down to a diameter of 10 cm in 2 cm steps, and the resulted reflection coefficients were measured at each bending step as shown in **Figure 4.4** (b). Slow motion camera was used to measure the restoration time against bending diameter down to 10 cm at 1 mm, 1.5 mm and 2 mm thickness.

4.5 Results and Discussions

The simulated 2D radiation patterns of the designed antenna were obtained by far field calculation in the software as shown in **Figure 4.3**, and the maximum gain was obtained 5.75 dBi at 2.4 GHz. The radiation patterns show that the proposed antenna is designed to get a high gain. The simulated elevation (E-plane) and azimuth (H-plane) radiation patterns are shown in **Figure 4.3** (a) and (b), respectively. To obtain these patterns, the proposed antenna in Figure 4.1 (a) is fabricated by using the design parameters as given in **Table 4.1**.

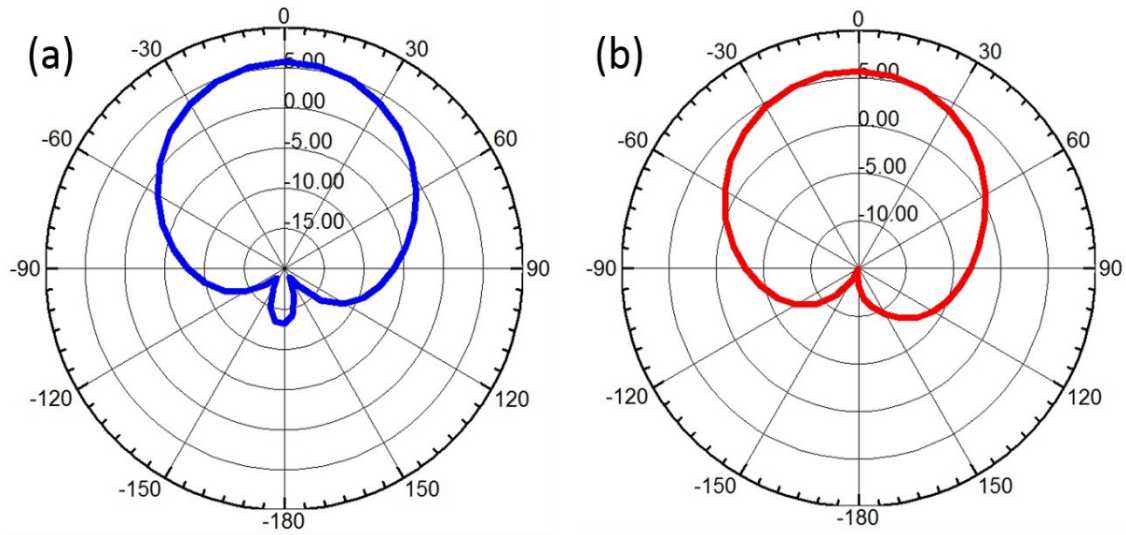

Figure 4.3. Simulated radiation patterns of the proposed inset microstrip patch antenna. (a) E-plane radiation pattern. (b) H-plane radiation pattern.

The VNA was utilized to measure the reflection coefficient of the fabricated antenna. The antenna was connected with vector network analyzer through coaxial cable and SMA RF connectors. **Figure 4.4** (a) shows that the measured reflection coefficient of the fabricated antenna is - 25.9 dB, whereas, the simulated value is - 31 dB. These results show good transmission from the antenna as the reflection coefficient (S_{11}) is less than -10 dB. This small value of - 25.9 dB was achieved by exploiting the inset feed line method for feeding the signal to the radiating patch. This result also indicates that the measured value follows the simulated value closely. The proposed antenna was characterized against bendability by flexing the antenna with hand and measuring S_{11} at each mechanical stress. The antenna was bent from straight (flat position) down to a diameter of 10 cm in a 2 cm step, and the results of S_{11} were measured at each bending step as shown in **Figure 4.4** (b). The effect of bendability resulted in a small shift of resonance frequency upward from 2.38 GHz to 2.44 GHz. The reflection coefficient varied from -24.5 dB to -18.5 dB under bendability of 2 cm to 10 cm. The maximum variation of S_{11} is 28.5% under these bending test, which indicates that the proposed antenna performance is not much affected under deformation to be used in wearable electronics.

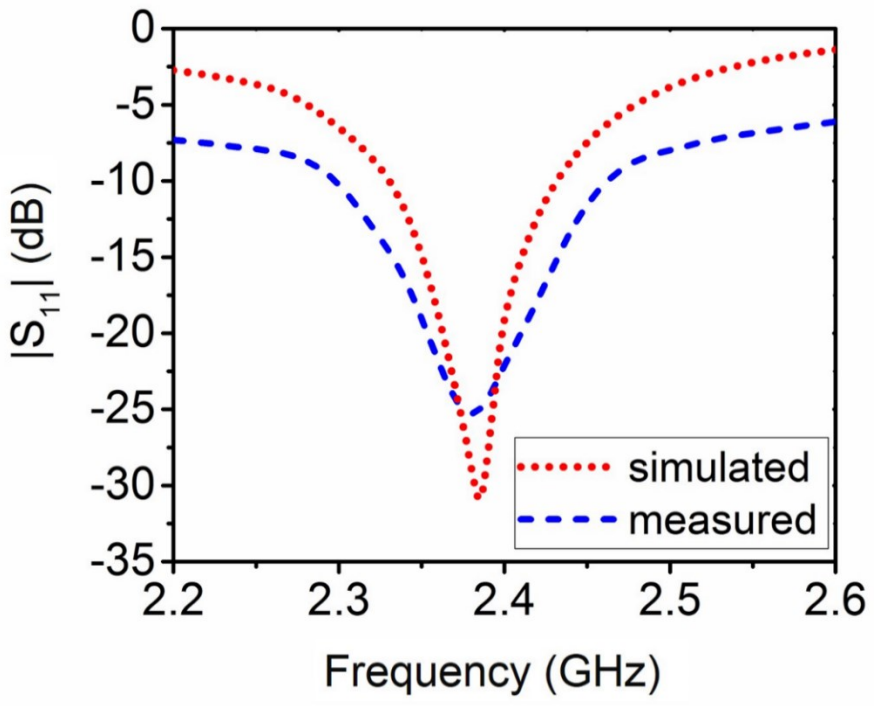

(a)

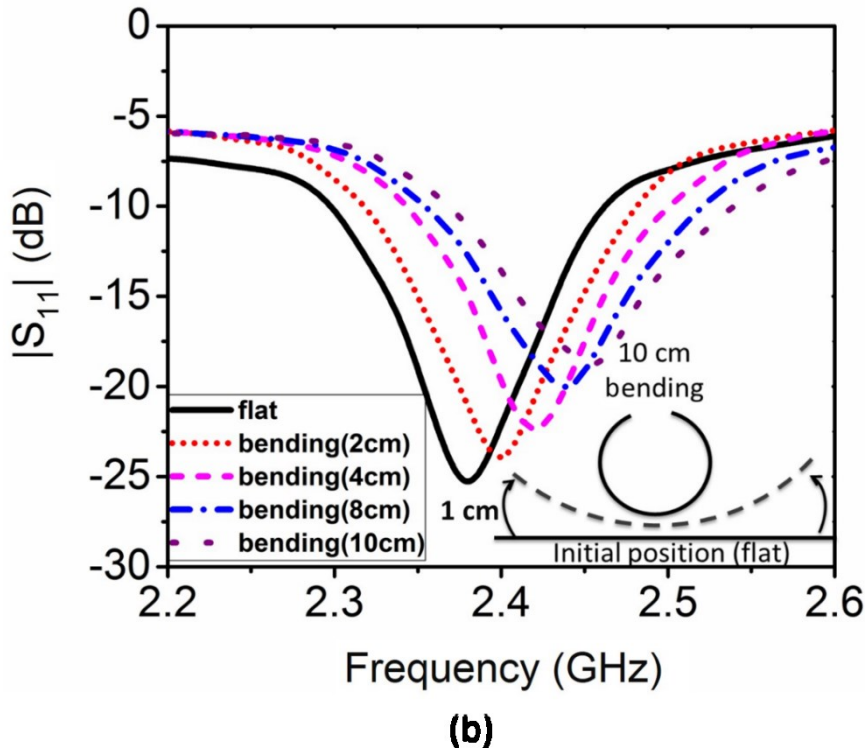

Figure 4.4. Reflection coefficient of the proposed antenna (a) Comparison of measured and simulated reflection coefficient. (b) Measured reflection coefficient along bending from 2 cm to 10 cm.

The optically transparency was verified by Shimadzu – UV/VIS/NIR-3150 spectrophotometer. **Figure 4.5** shows the optically transmission of the light from the proposed ITO/PDMS material antenna over different thickness. The spectrophotometer results show that the proposed antenna is transparent as the optical transmission approaches to 88% above wavelength 700 nm at the thickness of the antenna h = 1.5 mm. Above wavelength 700 nm, transmittance for h = 1 mm and h = 2 mm are 91.5% and 80%, respectively. Here, we can see that the value of the transmittance of the light increases as the thickness of the antenna decreases. These results suggest the proposed antenna can be sufficiently used in wearable electronic devices for transparent applications.

Slow motion camera was used to measure the restoration time against bending diameter down to 10 cm at 1 mm, 1.5 mm and 2 mm thickness. **Figure 4.6** shows the restoration (reformation to initial position) time is less than 210 ms which indicates that the antenna returns to its original position in a very short time after being released from deformation. It can be observed that at higher antenna thickness the restoration time is small but

degrades the optical transmission performance (as shown in **Figure 4.5**). Hence, there is trade-off between optical transmission and restoration time.

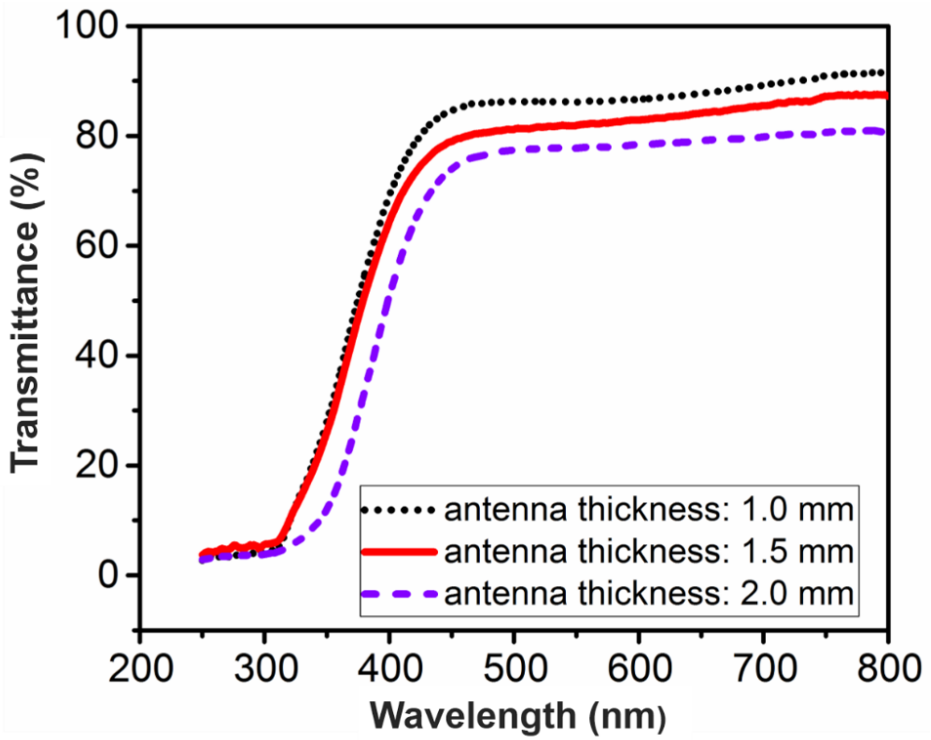

Figure 4.5. Transmittance of the light through the proposed antenna thickness measured by utilizing UV visible spectrophotometer.

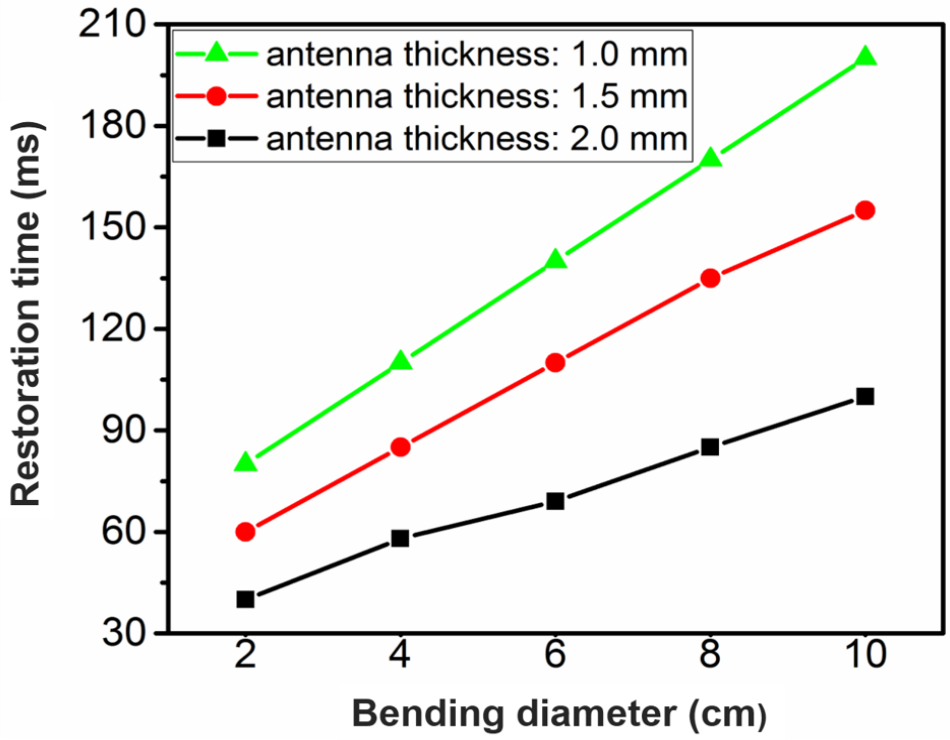

Figure 4.6. Restoration (to initial position) time vs bending diameter (as shown in inset of Figure 4.4).

4.6 Summary

We have demonstrated optically transparent and flexible antenna based on PDMS substrate and ITO radiating patch fabricated through commercialized inkjet material printing technology (DMP-3000) at ambient conditions. The fabricated antenna has been simulated in HFSS and characterized for S_{11} with vector network analyzer. The simulated S_{11} of dip point is -31 dB and a gain of 5.75 dBi whereas, the measured S_{11} is -25.9 dB and it reduced by 28.5% at 10 cm diameter bendability with reformation time less than 210ms. The proposed antenna showed transparency of 91.5%, 88%, and 80% at substrate thickness of 1 mm, 1.5 mm, and 2 mm, respectively. From these results, the proposed antenna is suitable for transparent and flexible wearable electronics operating at Wi-Fi 2.4GHz.

Chapter-5 RF Liquid Sensor

5.1 Introduction

RF and microwave techniques for sensing liquids are powerful and economical approaches to remotely detect and analyze liquid samples [65-67]. Among these approaches, measuring complex impedance of liquid samples as a function of frequency that provides information about relative dielectric constant and loss tangent of sample is widely used method, called dielectric spectroscopy. This method is used to characterize the relaxation time of various liquids such as petroleum, alcohol etc. and also analyzing biological samples that includes blood components, protein, DNA solution etc. [48-72]. Before this approach, optical and DC measurements were the popular methods for analyzing aqueous solutions. However, the optical method needs fluorescent labeling and the DC measurement provides limited information about the liquid contents [73]. Dielectric spectroscopy can provide the label free and missing information by integrating the microfluidic channels with the broadband transmission lines and metallic electrodes. The problem of using spectroscopy is that it needs complex design as well as expensive facilities to analyze the liquid samples by monitoring the dielectric constant over a wide range of frequencies. The microfluidic channels used in spectroscopy are also fabricated using laser etched method that is complex as well as expensive technology. Similarly, the analysis equipment is also costly and it does not provide remote monitoring solution [69]. The dielectric constant and impedance of liquid is a function of frequency [70]. Hence, by using microstrip technology we can monitor and analyze various liquid samples such as water, seawater, fresh water, ethanol and oils. In this approach, the resonance frequency of the microstrip patch structure depends upon the sample of liquid as different liquids have different chemical compositions so they have different dielectric constants.

Conventional manufacturing technology based on lithography can produce device with high accuracy [31]. However, this fabrication process is quite complicated, time consuming and requires precise control of temperature and pressure [3]. Other drawbacks are throughput limitations, lack of batch processing and use of rigid substrates and corrosive chemicals. Because of these issues, alternative fabrication methods have been

widely researched for microfluidics devices. Nowadays, inkjet-printed technology is very popular fabrication technique due to environment friendly, low-cost and low-temperature processing [33], [36]. Using this technology, we can easily fabricate low-cost and disposable electronic devices with single process in short time. An inkjet-printed microfluidic sensor for remote liquid analysis has been presented [74]. However, the minimum resonance frequency separation between liquids is relatively small, which makes it difficult to distinguish liquid correctly when small component or temperature change is present in the liquid. Furthermore, fabrication of the microfluidics channels requires complicated and expensive laser etching method [74-75]. Therefore, simple and low-cost RF sensor design having large resonance frequency separation is required.

In this paper, we proposed a simple radio frequency microstrip patch sensor to identify and monitor various liquids such as water, ethanol, water/ethanol 50:50 and synthetic engine oil. The microstrip sensor is designed in HFSS with lowest effective dielectric constant of 1.83 for empty case with 7mm substrate height. The sensor design has showed minimum resonance frequency separation of 80 MHz among liquids. For the best depth of reflection coefficients (good matching for all cases), design frequency analysis has been carried out and we have selected 1.6 GHz as it gave less than -25dB reflection coefficient value for all the cases. The HFSS designed microstrip patch sensor fabricated by commercial material inkjet DMP-3000 printer by depositing AgNPs on a glass substrate as radiator and ground. Both radiator and ground separated by empty chamber of 5 mm height, which can contain different liquid samples. We performed simulations and experiments, which confirmed that the resonance frequency of the structure changes according to liquid samples and we can remotely monitor this change. The measured resonance frequency of radiator patch with empty structure is 2.79 GHz, which lowers according to liquid type because dielectric constant of all liquids is high as compared to empty chamber case. The simple, handy and low cost fabrication with large resonance frequency separation makes the liquid sensor design attractive in fluidic monitoring and lab on chip applications.

5.2 Sensor Design

The design of the proposed radio frequency sensor consists of a conducting thin film of AgNPs based patch and a ground plane. The radiating patch and the ground separated by a glass substrate and chamber. In our design, we consider chamber as a part of substrate.

Thick substrates are effective for improving the impedance bandwidth but at the expense of increased radiator size. On the other hand, substrates with large dielectric constant can reduce the radiator size. However, the radiation efficiency deteriorates as these substrates concentrate electric field inside them. The charges accumulated at the edge of the microstrip patch create fringing field, which passes through the substrate and is reflected by the ground plane to reinforce the radiation. Therefore, it is desirable to have thick substrate with low dielectric constant to achieve better radiation efficiency [43]. Even though the substrate thick is used, liquid lowers radiation efficiency because of dielectric constant of the liquid. In microstrip patch design, there are many feed techniques like coaxial probe, aperture feeding, and proximity feeding and inset feeding [43]. We adopted inset microstrip feed line in order to have good input impedance match and simple on planar structure.

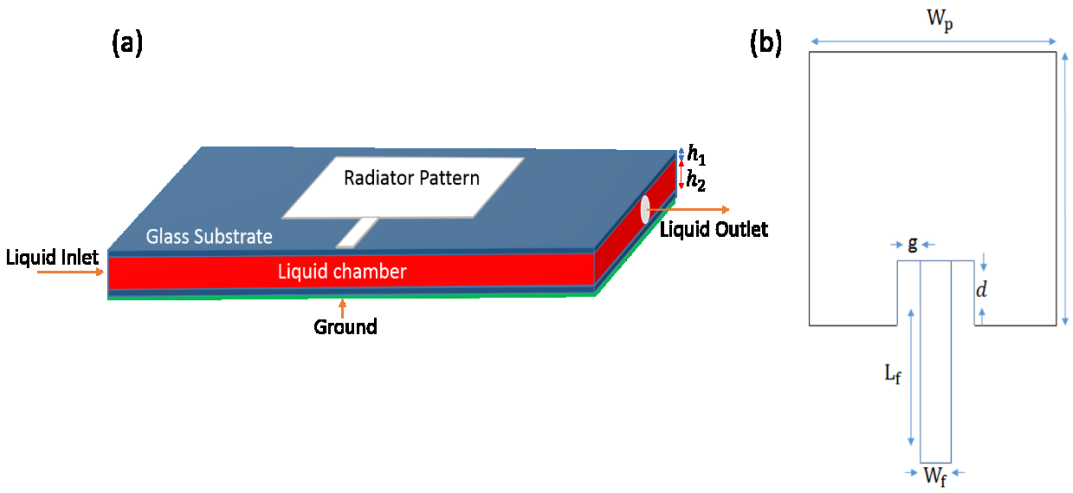

Figure 5.1. (a) Liquid sensor design. (b) Patch Radiator with parameters.

The proposed liquid sensor structure is as shown in **Figure 5.1** (a). The liquid inserted from liquid inlet passes through the chamber and drain out of the liquid outlet. From top to bottom, the configuration of the liquid sensor is composed of radiator pattern, glass substrate, liquid chamber, glass substrate and ground. The height of glass substrate and liquid chamber are represented by $h_1$and h_2, respectively. The radiator pattern design with all parameters is shown in **Figure 5.1** (b), where W_p and L_p are the width and length of the patch radiator respectively. The width and length of the inset feed line in the patch radiator are shown by W_f and L_f respectively. The notch width and inset depth represented by g and d respectively, are symmetric along the width of the patch radiator.

We set design strategy having large frequency separations between adjacent liquids and reflection coefficient lower than -25 dB for all liquids. The proposed design steps are as follows:

1. Selection of effective dielectric constant (ε_{reff}): The dielectric constants (ε_r)of glass, empty chamber, water and ethanol at room temperature are 5.5, 1, 81 and 24, respectively. By using these dielectric constants, we calculated the ε_{reff} of three layers composed of glass, liquid and glass [76]. The ε_{reff}s of empty chamber, oil, ethanol and water cases are 1.83, 2.23, 2.69 and 2.73, respectively. We designed and simulated four sensors by using four ε_{reff}s and obtained best ε_{reff} giving best frequency separation. Since the lowest ε_{reff} has better radiation efficiency, the design with lowest ε_{reff} has good response [43]. Thus, we have selected $\varepsilon_{reff} = 1.83$.
2. Selection of substrate height: We analyzed reflection coefficient according to total substrate height ($h_1 + h_2 + h_1$) as shown in **Figure 5.2**. By keeping the height of the glass (h_1) as 1mm we changed height of liquid chamber (h_2) and obtained that total height of 7 mm showed lowest reflection coefficient. Therefore, we have selected 7mm as height of substrate.

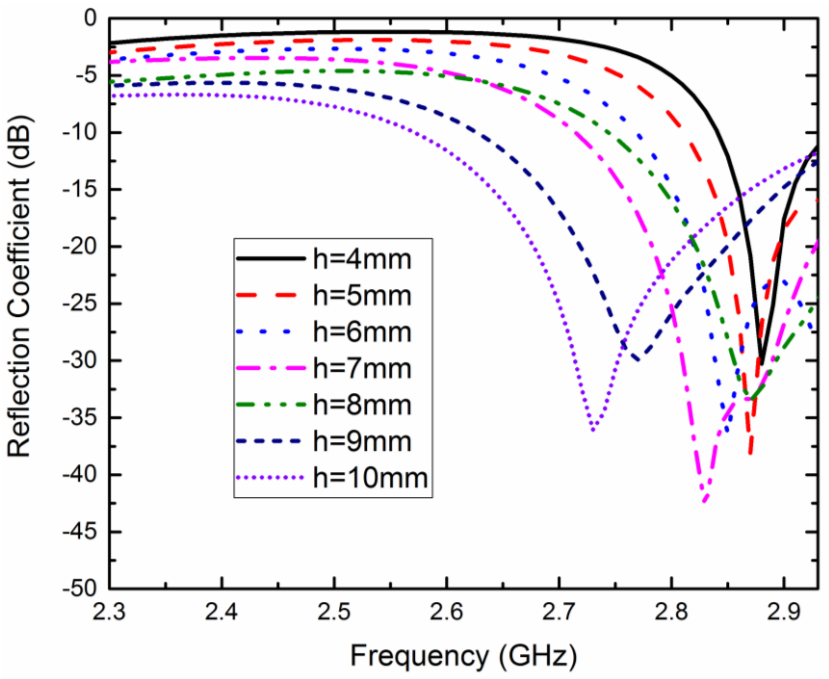

Figure 5.2. Reflection coefficient analysis of the sensor against substrate height.

3. Selection of design frequency (f_r): Initially, we considered empty chamber with ε_{reff} of 1.83. Next, we analyze designs obtained by changing frequencies and select the best design frequency giving reflection coefficient under -25dB for all liquids. Note that changes of the design frequency causes impedance change, which results in changes of reflection coefficients. For analysis, we used 1.2GHz as starting frequency for the empty case. The length of patch causes change of resonance frequency, which obeys the following:

$$f_r = \frac{nc_0}{4\,(\mathrm{L} + \mathrm{L_o})\,\sqrt{\varepsilon_{reff}}} \qquad [1]$$

, where c_0 is the speed of light, n is the resonance mode of the design and $\mathrm{L_o}$ is the correction factor due to fringing electric field. We start design for empty chamber (ε_{reff} of 1.83) with initial 1.2GHz resonance. Then, we fill all the liquids in the chamber and obtain reflection coefficients and resonance separations between liquids. Next, we design for empty chamber with 1.25 GHz resonance and obtain reflection coefficients and resonance separations. The results up to 1.7GHz are as shown in **Figure 5.3** (a) and (b), which show the minimum, average and maximum reflection coefficients and resonance separations. Based on these results, we chose design frequency of 1.6 GHz that satisfies both large resonance separation and reflection coefficient under -25dB for all liquids. The obtained liquid sensor parameters are shown in Table 5.1.

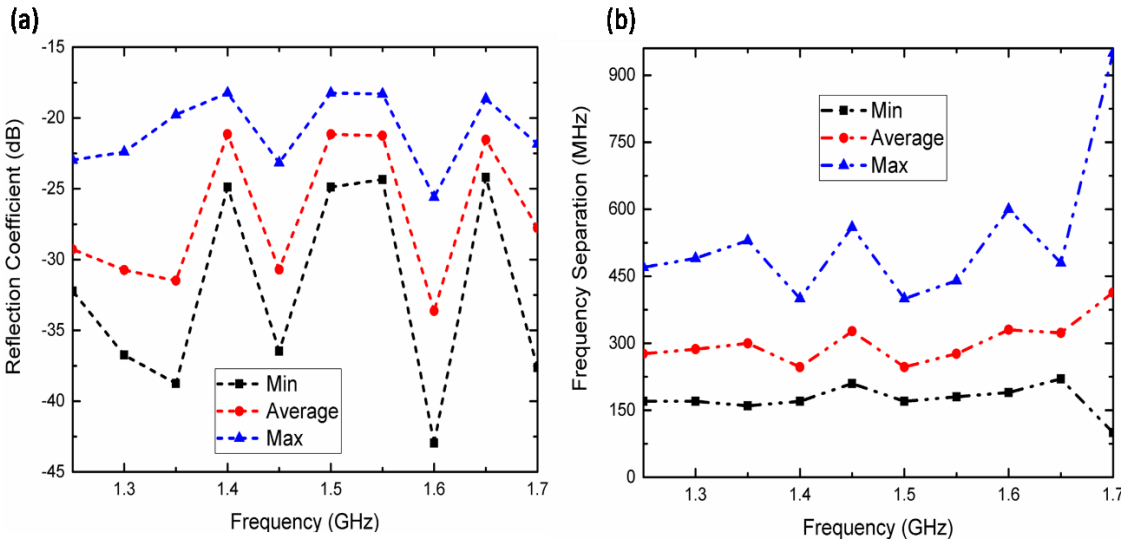

Figure 5.3. (a) Reflection coefficient analysis of the sensor against design frequencies showing minimum, average and maximum reflection coefficients of consider liquids water, ethanol, oil and empty case. (b) Minimum, average and maximum frequency separation among the considered cases water, ethanol, oil and empty for different design frequencies.

Table 5.1. Design parameters of the proposed antenna.

Parameter	Dimension (mm)	Parameter	Dimension (mm)
g	15.55	d	18.65
W_p	78.8	W_f	31.11
L_P	62.5	L_s	194.9
h_1	1.00	L_f	61.55
W_s	172	h_2	5

By using these parameters, we have used HFSS for full wave analysis of the proposed sensor design. By sweeping frequency from 1400 MHz to 3 GHz, we obtained reflection coefficients (S_{11}) according to water, air, synthetic engine oil, ethanol and water/ethanol 50:50, which are as shown in **Figure 5.4**. We can observe that the proposed design satisfy the requirement of reflection coefficient with large separations. The reflection coefficient of empty case shows clear -42.95 dB dip point at 2.83 GHz, which indicates load impedance of the design matches well with the empty case. For the oil case, the resonance frequency is 2.63 GHz with reflection coefficient of -34.80dB. For the ethanol and water cases, their resonance frequencies are 2.03GHz and 1.84GHz and reflection coefficients are -25.59dB and -31.19dB, respectively. The frequency separation between empty and oil cases is 200 MHz and is 190 MHz between water and ethanol cases. The obtained 190MHz frequency separation is greater than previous design [75] showing 50MHz separation for ethanol and water case. The frequency separation for oil and ethanol is 600MHz. For mixture of water and ethanol by 50:50, we obtained 1.92 GHz resonance frequency and the reflection coefficient of -30.18dB. The resonance frequency separations of mixture of water and ethanol to ethanol and to water are 110MHz and 80MHz, respectively. Note that liquid with lower effective dielectric constant has higher resonance frequency.

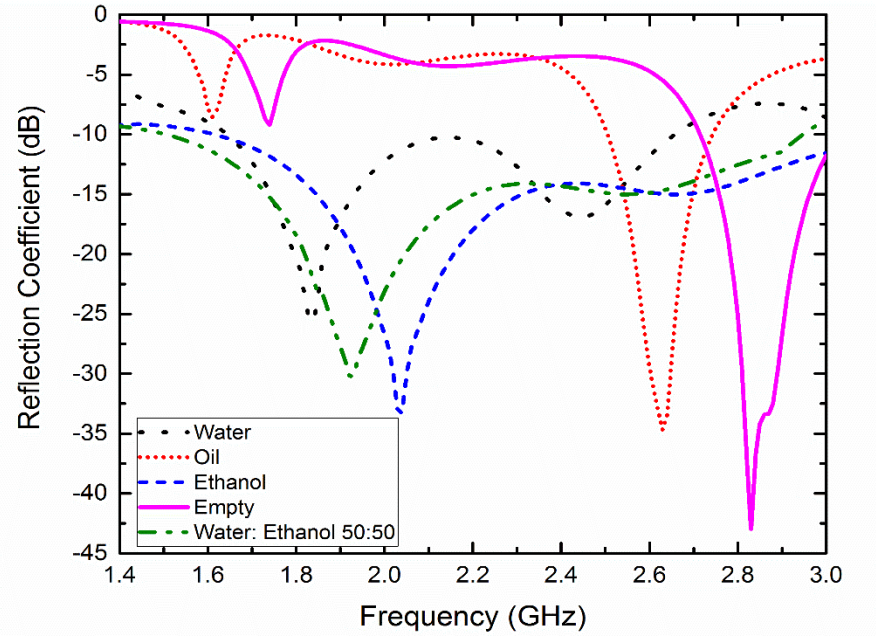

Figure 5.4. Reflection coefficient of the proposed sensor with water, ethanol, oil, empty and water/ethanol 50:50 mixture.

5.3 Sensor Fabrication and Characterization

To fabricate the sensor, we export the verified design to inkjet-printing. The AgNPs ink (purchased from Sigma Aldrich South Korea) filled into 10pL cartridge of 16-jet nozzles with diameter of 9 µm and distance of 254 µm for high resolution and non-contact jetting. The inkjet-printing setup, for the metallization and ground layer is DMP-3000 material deposition printer as shown in **Figure 5.5**. The printing parameters such as drop spacing of 25 µm, jetting frequency of 5 kHz, cartridge nozzles voltage of 25 V and printer hot platen temperature of 40 °C adjusted by printing software Dimatix Drop Manager (DDM). We used (200 mm ×200 mm × 1) glass substrate purchased from Sigma Aldrich, South Korea. We cut the glass substrate according to the required dimensions with cutting machine. The surface of a glass is usually rough with scratches and contaminated by some organic materials, so before printing we cleaned it with ethanol baths at ambient condition, rinsed it with water and dried it at 40 °C for 3 minutes. To achieve low film resistance of radiator pattern, three metallization layers of radiator pattern printed on glass substrate and then treated with hot plate for 2hr minutes at 40 °C. The conductive ground pattern printed on the glass substrate by adopting same procedure as used for the printing of radiator pattern. After curing both patterns on the glass substrates, the spacer (with already containing inlet and outlet for liquid) was attached at the edges of one glass

substrate with glue and then second glass in placed on top of the spacer and it was also glued. Small tubes according to the size of inlet and outlet are inserted and glued. For feeding signal, we attached subminiature version A (SMA) to the inset feed line by using sliver epoxy paste and soldering. The consequent radio frequency liquid sensor is shown in **Figure 5.6** (a) and (b).

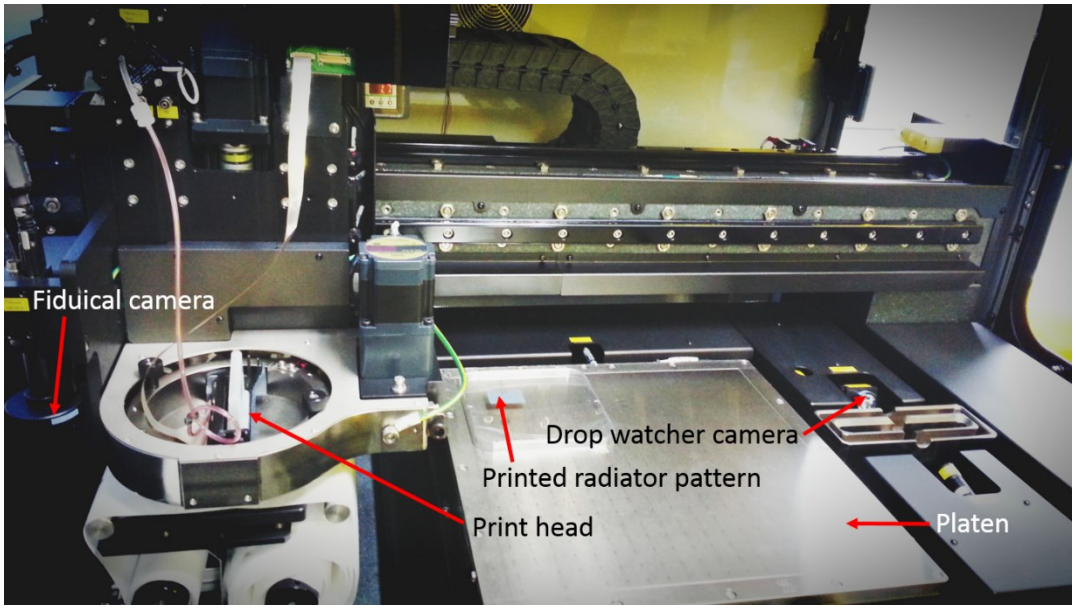

Figure 5.5. Printing setup of Dimatix Material Printer (DMP-3000).

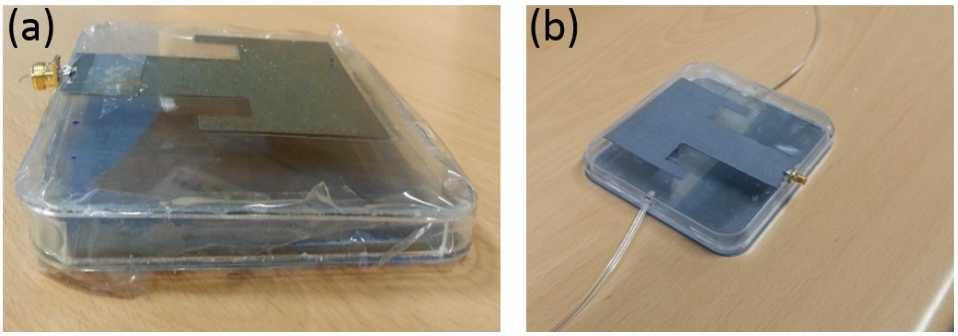

Figure 5.6. (a) Fabricated radio frequency liquid sensor. (b) Sensor with inlet and outlet.

In order to characterize surface morphology of the proposed sensor, we used the NV-2000(Universal), non-contact 3D surface profiler of nanoscale precision. By using phase shifting interferometry (PSI) mode in the profiler, we obtained 3D profile of silver radiator pattern over glass substrate, as shown in **Figure 5.7** (a). It can been seen that the silver pattern is uniformly deposited with thickness of 351 nm. The electrical

conductivity of Ag film is 4×10^6 S/m, whereas the copper with the same thickness has electrical conductivity of 5×10^6 S/m, which is relative comparable to Ag film [64]. The electrical conductivity of the Ag film increases with increasing the thickness. The radiation efficiency of the radiator is better if the electrical conductivity of the Ag film is high and vice versa. By using the Jeol JSM-7600F, we subsequently obtained scanning electron microscopy (SEM) image of silver radiator pattern with 10µm scale, as shown in **Figure 5.7** (b). We can observe uniformly deposited silver layer over the glass surface.

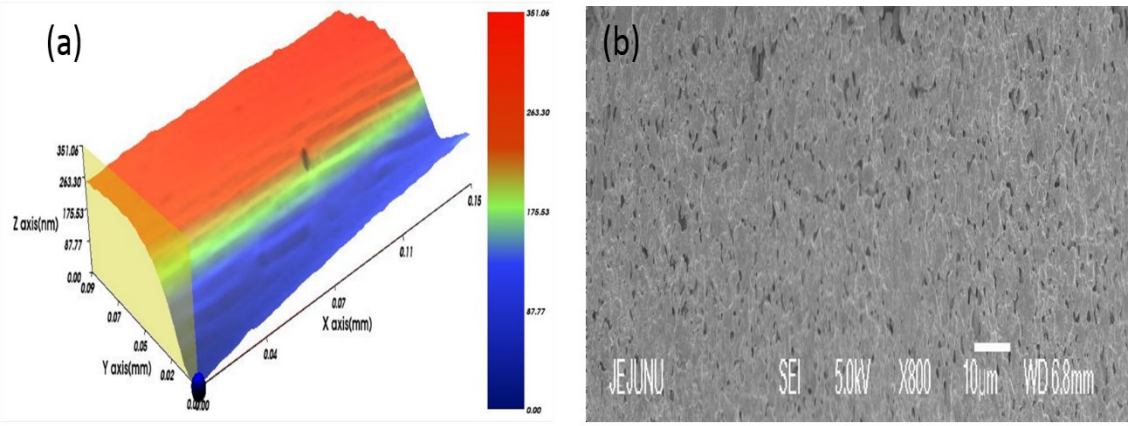

Figure 5.7. (a) 3D nano profile of liquid sensor. (b) SEM image of the printed silver ink pattern.

5.4 Results and Discussions

To observe the resonance frequency shifting, we characterized the printed antenna by using calibrated HP VNA connected with 50Ω transmission line and 50Ω RF SMA connector. By using the experimental setup shown in **Figure 5.8** (a), we measured reflection coefficients over frequency range of 1400 MHz to 3 GHz, as shown in **Figure 5.8** (b). We can observe that the measured reflection coefficients agree with the HFSS simulation results in Figure 5.4. Measured resonance frequency for empty case is 2.79 GHz with reflection coefficient of -40.15dB and the resonance frequency is shifted to 1.79 GHz with reflection coefficient of -29.8 dB for water case. We can observe similar trend in Figure 5.4, in which the resonance frequency is shifted from 2.83 GHz to 1.83 GHz for water case. We think resonance frequency differences is due to fabrication error. However, as we expect, resonance frequency decreases when chamber filled with water of which relative dielectric constants is 80. In case of water chamber, most of electric

field resides inside substrate so that radiation efficiency decreases. On the other hand, the radiation efficiency is high in case of empty chamber because air inside the chamber assures more radiation in air.

Next, we tested different liquids such as synthetic engine oil, ethanol and water/ethanol 50:50. As shown in **Figure 5.8**, the resonance shifts according to liquid type. The resonance depends on the dielectric constant as it can change the capacitance between two conductive plates and also the impedance of the structure changes that results in change of resonance [43].

Table 5.2. Summary of measured highest dip point frequency (GHz) and reflection coefficient (dB) for various liquids

Terms	Water/Ethanol 50:50	Water	Ethanol	Synthetic Engine Oil	Empty
f_{rs}(GHz)	1.92	1.84	2.03	2.63	2.83
f_{rm}(GHz)	1.93	1.79	2.19	2.59	2.79
$\lvert f_{rs} - f_{rm} \rvert$ (MHz)	10	50	160	40	40
$\lvert \Delta f_{rs} \rvert$ (MHz)	80	190	600	200	N/A
$\lvert \Delta f_{rm} \rvert$ (MHz)	140	400	400	200	N/A
$\lvert \Delta f_{rm} \rvert$ (MHz) B. S. Cook [75]	N/A	36	52.85	N/A	N/A
Measured null depth (dB)	-32.75	-29.8	-34.10	-36.5	-40.15
Measured null depth (dB) B. S. Cook [75]	N/A	-42.5	-22.8	N/A	-31

The results are summarized in **Table 5.2**, where simulated and measured resonant frequencies of liquids are represented by f_{rs} and f_{rm} respectively. We denote the

difference between these frequencies as $|f_{rs} - f_{rm}|$ in MHz. Also, we represent the frequency difference between two successive simulated and measured resonance frequencies as $|\Delta f_{rs}|$ and$|\Delta f_{rm}|$, respectively. For example, the f_{rs}s of water/ethanol 50:50 and water are 1.92 GHz and 1.84 GHz, respectively so the $|\Delta f_{rs}|$ becomes 0.08GHz. Similarly, $|\Delta f_{rm}|$ can be calculated and the results are summarized in **Table 5.2**.

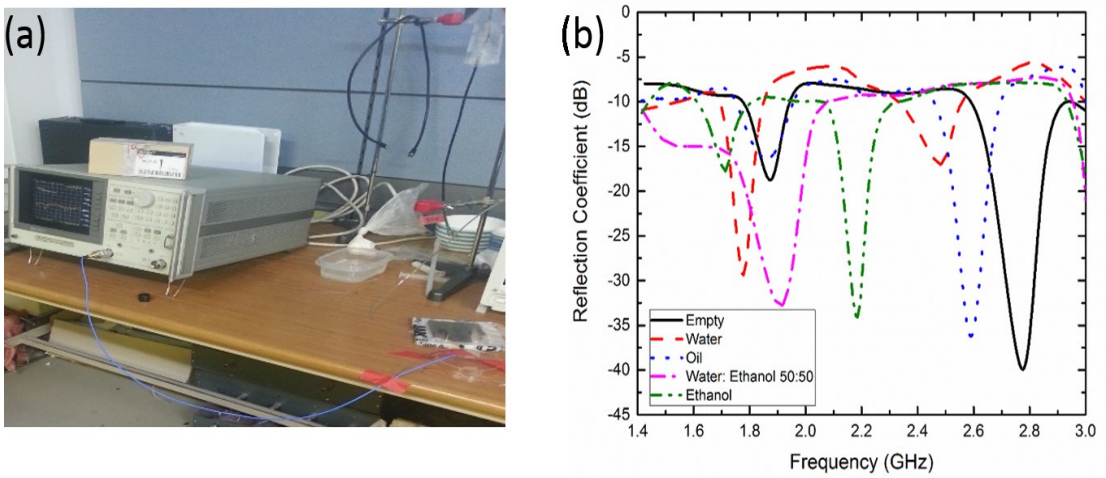

Figure 5.8. Reflection coefficient of various liquids over 1.4 GHz to 3 GHz range and inset shows the experimental setup for measurement using vector network analyzer.

5.5 Summary

We have demonstrated a low cost microstrip sensor for liquid detection. The proposed sensor has been designed to achieve low under -25dB reflection coefficient and large resonance separation among the considered liquids. The sensor can easily identify different liquids as the minimum $|\Delta f_{rm}|$ was 140 MHz among the liquids. The resonant frequency for empty chamber case was recorded 2.79 GHz and it has showed dependent behavior according to liquid type. Water, ethanol, water/ethanol 50:50 and synthetic engine oil have showed resonant frequencies of 1.78, 2.19, 1.93 and 2.59 GHz respectively. These results suggests that the proposed liquid sensor can detect liquid type and it can be used in various liquid sensing and lab on chip applications. Especially, for maintaining the quality of liquids such as water and oil.

Chapter 6 Conclusions and Future Work

This brief chapter describes the overall conclusions of the dissertation and highlights the contribution made in the RF flexible printed antennas and sensors.

6.1 Overview and General Conclusions

In last decade, printed electronics is emerged as a new technology that full fills the missing gap associated with conventional vacuum based techniques with dynamic style by enabling low profile, light weight, inexpensive, easy fabrication of small and large area devices. Currently, the flexible wearable printed electronics is an attractive research topic that tops the pyramid of research in both academia and industry as well. The next generation electronics requirements such as low-cost, flexible and low temperature processing are encouraging the researchers and industry to work in this emerging branch of electronics.

In order to communicate these printed electronics circuits and systems flexible antenna are integral part of these printed electronic systems. As printed electronics is relatively new field, hence fabrication of the antenna device and its integration is challenging. In past decade, a lot of efforts have been made in term of functional materials which are deposited for patterning. Apart from the material investigation for the flexible printed antennas, fabrication techniques are also under study. Among them, few fabrication techniques are matured such inkjet and EHD. Hence, these are adopted by the electronic industry. In this thesis work Inkjet printing technique is used for the fabrication of antennas and RF sensor as it is reliable printing technique. The device are fabricated and tested to confirm their characteristics and performance. This thesis contributes to the Research and Development (R&D) community to address the challenges in the fabrication process on thin and thick transparent substrates of flexible all-printed antenna for wearable printed electronic applications and RF printed sensor for liquid identification. Main contributions are listed as under:

1. Printed and flexible antenna is presented for 1.8GHz band applications by depositing AgNPs based radiating element through commercial Dimatix material inkjet printer on a 0.04mm thin, transparent and flexible PET substrate. The antenna is designed and simulated in FEM based Ansys HFSS and, the achieved reflection coefficient, gain and efficiency of the antenna are -23dB, 2.72dBi and 93.33%, respectively. The resonance frequency of the antenna is confirmed by NI Multisim simulation on equivalent circuit of antenna design. The antenna is characterized by VNA and spectrum analyzer. The measured S_{11} and -10dB bandwidth are -32.2dB and 190.5MHz, respectively. The compact design based on thin, transparent and fully bendable PET substrate, makes the design attractive since it can overcome limits of cost and size. These results suggests that the presented all-printed is suitable candidate for electronic devices operating over 1.8 GHz band such as Telos-B and other wearable printed devices.

2. High gain antenna operating over dual band of 900MHz and 2.4GHz is designed in HFSS and fabricated by using commercial DMP-3000 and AgNPs conductive ink to print the antenna pattern on 50-micron thin, transparent and flexible PET substrate. The VNA characterization showed reflection coefficients of -16.4dB at 900MHz and -26dB at 2.4GHz, which accord with the FEM based HFSS simulation results. HFSS results showed antenna gains as high as 16.74dBi and 16.24dBi at 900MHz and 2.4 GHz, respectively and 23.33% and 11.66% of -10dB fractional bandwidth at 900MHz and 2.4GHz, respectively. These results suggest that the presented high gain antenna can be used for dual band Wi-Fi communication and wearable printed electronics devices as well.

3. A transparent and flexible inset-microstrip patch antenna for 2.4 GHz wearable printed electronics applications is introduced. The presented antenna is designed in Ansys HFSS and realized by depositing transparent ITO nanoparticles as a radiating patch and a ground on the flexible and transparent PDMS substrate by utilizing Fujifilm Dimatix inkjet material printer DMP-3000 at ambient conditions. On a flat position, the simulated gain of the

presented antenna is 5.75 dBi, and its measured reflection coefficient is -25.9 dB. During bendability test; down to a diameter of 10 cm, the reflection coefficient is decreased up to 28.5%. The transparent antenna design showed the transparency of 91.5%, 88% and 80% at thickness of 1 mm, 1.5 mm and 2 mm, respectively, and its restoration time is recorded that is not more than 210 ms.

4. A compact RF microstrip patch sensor is demonstrated for liquid identification. The relationship between the dielectric constant and resonance frequency provides the liquid sensing mechanism. The RF liquid sensor is composed of radiator and ground fabricated by AgNPs ink on a transparent glass substrate and separated by empty chamber of 5 mm height for containing liquid sample. A simple design procedure is presented, to find out not only, maximum frequency separation between two adjacent resonance frequencies but, also lowest reflection coefficients at the resonance frequencies. Low cost, fast and environmentally friendly inkjet printing technique is used for sensor fabrication. The fabricated sensor has 140 MHz minimum frequency separation and maximum -29dB reflection coefficient, which gives large identification margin.

6.2 Future Work

At the end of each chapter there is summary of the section where the achieved performance of antennas and sensor is discussed with their numerical values. The antenna design and its performance is improved by mean of fabrication technique, fabrication process or by material as the comparison tables are shown in respective chapters. In future, these printed flexible antennas and liquid RF sensor can be investigated for better performance and reliability. Specifically, the printed antennas on various transparent substrates with different conductive materials can be improved for high transparency, high gain, high efficiency, better radiation and bandwidth characteristics. Apart from the performance improvement, the integration of antenna with large systems and exiting CMOS technology is still an issue for real time printed electronics applications. The printed RF sensor can be improved in term of their

compact design and to achieve more resolution to distinguish and identify minute change in liquids such as to differentiate the normal diesel and ship diesel with high reliability is still a challenging task for RF liquid sensor.

Annex-A Journal Papers

1. **Arshad Hassan**, Shawkat Ali, Jinho Bae* and Chong Hyun Lee: *All printed antenna based on silver nanoparticles for 1.8 GHz applications.* Applied Physics A, 2016, Vol. 122, 768. DOI:10.1007/s00339-016-0286-2

2. **Arshad Hassan**, Shawkat Ali, Gul Hassan,Jinho Bae* and Chong Hyun Lee: *Inkjet-printed antenna on thin PET substrate for dual band Wi-Fi communications* Micro system Technologies· August 2016. DOI: 10.1007/s00542-016-3113-y.

3. **Arshad Hassan,** Shawkat Ali, Jinho Bae, Chong Hyun Lee: *Inkjet printed transparent and bendable patch antenna based on polydimethylsiloxane and indium tin oxide nanoparticles*. Microw. Opt. Technol. Lett. , 2016, 58: 2884–2887. DOI:10.1002/mop.30171

4. **Arshad Hassan,** Kibae Lee, Jinho Bae, Chong Hyun Lee: *An Inkjet-Printed Microstrip Patch Sensor for Liquid Identification*. Sensor and Actuator A. November 2017. DOI: https://doi.org/10.1016/j.sna.2017.11.028

5. Shawkat Ali, **Arshad Hassan,** Gul Hassan, Jinho Bae, Chong Hyun Lee: *All-Printed humidity sensor based on graphene/methyl-red composite with high Sensitivity.* Carbon, 2016, 105, 23-32. DOI:10.1016/j.carbon.2016.04.013

6. Gul Hassan, FasiUllah khan, **Arshad Hassan**, Shawkat Ali, Jinho Bae, Chong Hyun Lee: *A flat-panel-shaped hybrid piezo/triboelectric nanogenerator for ambient energy harvesting*. Nanotechnology. Apr 2017, 28(17):175402. DOI: 10.1088/1361-6528/aa65c3.

7. Shawkat Ali, **Arshad Hassan,** Jinho Bae, Chong Hyun Lee: *Printed differential temperature sensor for the compensation of bending effect.* Langmuir, 2016, 32 (44), 11432–11439. DOI: 10.1021/acs.langmuir.6b02885

8. Shawkat Ali, **Arshad Hassan,** Gul Hassan, Jinho Bae, Chong Hyun Lee: *Flexible Frequency Selective Passive Circuits Based on Memristor-Capacitor*. Organic Electronics, 2017, 51, 119-127. DOI: https://doi.org/10.1016/j.orgel.2017.09.012

Annex-B to be Submitted Papers

1. Shawkat Ali, **Arshad Hassan**, Gul Hassan, Chang-Ho Eun, Jinho Bae, Chong Hyun Lee and In-Jung Kim: *Disposable all-printed electronic biosensor for instantaneous detection and classification of pathogens;* Scientific reports (Submitted)

2. Kibae Lee, **Arshad Hassan**, Chong Hyun Lee, Jinho Bae: *Microstrip Patch Sensor for Salinity Determination;* Sensors (submitted)

3. Gul Hassan, Jinho Bae, **Arshad Hassan**, Shawkat Ali, Chong Hyun Lee and Yohan Choi, *Ink-jet Printed Stretchable Strain Sensor Based on Graphene/ZnO Composite on Micro-random Ridged PDMS Substrate*; Composite part A. (submitted)

4. Gul Hassan, Jinho Bae, Chong Hyun Lee and **Arshad Hassan**, *Wide Range and Stable Ink-jet Printed Humidity Sensor Based on Graphene and Zinc Oxide Nanocomposite;* Journal of Materials Science: Materials in Electronics (Submitted)

Annex-C Conference Papers and Posters

1. **Arshad Hassan**, Shawkat Ali, Jinho Bae, Kyung Hyun Choi, Chong Hyun Lee: *Flexible dual-band antenna for communication and radar applications*. 2016 IEEE Radar Conference At Philadelphia, PA, USA. DOI: 10.1109/RADAR.2016.7485255

2. **Arshad Hassan,** Shawkat Ali, Gul Hassan, Jinho Bae, Chong Hyun Lee: *Microfluidics-Based Tunable Printed Coplanar Waveguide Monopole Sensor*. Proceedings of ISERD International Conference, Rawalpindi, Pakistan, 29th-30th March 2017, 4-6, ISBN: 978-93-86083-34-0.

3. Shawkat Ali, **Arshad Hassan**, Gul Hassan, Jinho Bae, Chong Hyun Lee: *Memristor-capacitor passive filters to tune both cut-off frequency and bandwidth*. 25th International Conference on Optical Fiber Sensors, Jeju, South Korea. DOI: 10.1117/12.2264963

4. Gul Hassan, Shawkat Ali, **Arshad Hassan**, Jinho Bae, Chong Hyun Lee: *FSK Modulation Based on Pedot: PSS and Methyl Red Heterojunction Memristor.* ISERD International Conference, Rawalpindi, Pakistan, 29th-30th March 2017, 1-3, ISBN: 978-93-86083-34-0.

5. Syed Saad Ali, **Muhammad Arshad Hassan Khan**: Extraction of Strongest Multipath Using Principal Component Analysis. MDSRC - 2015 Proceedings, 14-15 November, 2015 Wah/Pakistan.

6. **Arshad Hassan**, Jinho Bae, Chong Hyun Lee: All-printed L-band antenna based on silver nanoparticles. 24th-26th June 2017, 1C-4, Joint Symposium of Jeju National University and Nagasaki University on Science and Technology JSST 2017.

7. Shawkat Ali, Jinho Bae, Gul Hassan, **Arshad Hassan**, and Chong Hyun Lee: Flexible Light Emitting Device Based on Resistive Switching to Memorize Light State. 21-22 February 2017, London, Uk, Global Engage Printed and Flexible Electronics Congress 2017, http://www.global-engage.com/event/printed-flexible-electronics/

8. Gul Hassan, Jinho Bae, Shawkat Ali, Chong Hyun Lee, **Arshad Hassan**, and Yohan Cho: High Stretchable Strain Sensor fabricated on Micro-Randomly Ridged PDMS Substrate Using Graphene/ZnO Composite. 21-22 February 2017, London, Uk, Global Engage Printed and Flexible Electronics Congress 2017, http://www.global-engage.com/event/printed-flexible-electronics/

Bibliography

[1] A. Nathan et al., Proc. IEEE 100, 1486 (2012).

[2] R. M. Pasqualrelli et al., Chem. Soc. Rev. 40, 5406 (2011).

[3] S. Ali, J. Bae, and C. H. Lee, Applied Physics A 119 (4), 1499 (2015)

[4] H. Khaleel, Innovation in Wearable and Flexible Antennas, Billerica, MA, USA:WIT Press, 2014

[5] Minhun Jung et al., IEEE Transactions on Electron Devices 57 (3), 571 (2010) DOI: 10.1109/TED.2009.2039541

[6] Graphene Flagship. Graphene technology enables fully flexible NFC antennas. Science Daily. www.sciencedaily.com/releases/2016/11/161129084229.htm (accessed December 12, 2017).

[7] R. Waterhouse, D. Novak, and G. Burnie, Military Communications Conference, pp. 1–6 (2006).

[8] H. R. Khaleel, IEEE Transactions on Components, Packaging and Manufacturing Technology 4 (10), 1722 (2014).

[9] DMP-3000 Materials printer manual.

[10] H. Park, H. Kang, Y. Lee, Y. Park, J. Noh, G. Cho, Nanotechnology 23, 344006 (2012).

[11] D. Sung, A. De La Fuente Vornbrock, V. Subramanian, IEEE Trans. Compon. Packag. Technol. 33, 105 (2010).

[12] B. O. Choi, C. H. Kim, D. S. Kim, Proc. Inst. Mech. Eng. Part C 224, 149 (2010).

[13] R. Zichner, F. Siegel, M. Hösel, R. R. Baumann, Proc. LOPE-C 13 (2010).

[14] D. Brown, SMT Mag. 20, 28 (2006).

[15] C. Waldschmidt, S. Schulteis, W. Wiesbeck, IEEE Trans. Vehic. Technol. 53, 579 (2004).

[16] R. Zichner, R. R. Baumann, Adv. Radio Sci. 9, 401 (2011).

[17] L. B. Wang, K. Y. See, B. Salam, A. C. W. Lu, J. W. Zhang, S. Tengiz, Proc. APEMC 661 (2012).

[18] R. Zichner, F. Siegel, R. R. Baumann, Proc. LOPE-C 361 (2011).

[19] T. R. Andersen, T. T. Larsen-Olsen, B. Andreasen, A. P. L. Böttiger, J. E. Carlé, M. Helgesen, E. Bundgaard, K. Norrman, J. W. Andreasen, M. Jorgensen, F. C. Krebs, ACS Nano 5, 4188 (2011).

[20] E. Sowade, J. Hammerschmidt, T. Blaudeck, R. R. Baumann, Adv. Eng. Mater. 14, 98 (2012).

[21] R. R. Baumann, A. Willert, T. Blaudeck, Proc. iarigai 327 (2010).

[22] M. Hösel, R. R. Søndergaard, M. Jørgensen, F. C. Krebs, Adv. Eng. Mater. 15, 1068 (2013).

[23] A. Willert, R. R. Baumann, IEEE ISCDG 1 (2013).

[24] H. A. D. Nguyen, J. Lee, C. H. Kim, K.-H. Shin, D. Lee, J. Micromech. Microeng. 23, 095010 (2013).

[25] J. So, J. Thelen, A. Qusba, G. J. Hayes, G. Lazzi, M. D. Dickey, Adv. Functional Mat. 19, 3632 (2009).

[26] R. Zichner, R. R. Baumann, Jpn. J. Appl. Phys. 52, 05DC24 (2013).

[27] D. E. Anagnostou, A. A. Gheethan, A. K. Amert, K. W. Whites, J. Disp. Technol. 6, 558 (2010).

[28] S. H. Choi, T. J. Jung, S. Lim, Electronics Lett. 46, 1181 (2010).

[29] A. A. Gheethan, D. E. Anagnostou, IEEE Trans. Antennas and Propag. 60, 2071 (2012).

[30] H. R. Khaleel, H. M. Al-Rizzo, D. G. Rucker, IEEE Disp. Technol. 8, 91 (2012).

[31] L. Yang, A. Rida, R. Vyas, M. M. Tentzeris, IEEE Trans. Microw. Theory Techn. 55, 2894 (2007).

[32] L. Song, A. C. Myers, J. J. Adams, Y. Zhu, ACS Appl. Mater. Interfaces 6, 4284 (2014).

[33] T. Sekitani, K. Zaitsu, Y. Noguchi, K. Ishibe, M. Takamiya, T. Sakurai, and T. Someya, IEEE Trans. Electron Dev. 56, 1027 (2009).

[34] S. R. Forrest, Nature 428, 911 (2004).

[35] T. Sekitani, T. Yokota, U. Zschieschang, H. Klauk, S. Bauer, K. Takeuchi, M. Takamiya, T. Sakurai, and T. Someya, Science 326, 1516 (2009).

[36] E. Cantatore, T.C. Geuns, G.H. Gelinck, E. van Veenendaal, A.F. Gruijthuijsen, L. Schrijnemakers, S. Drews, D.M. de Leeuw, IEEE J. Solid-state circuits 42, 84 (2007).

[37] http://members.tm.net/lapointe/Plastics.htm

[38] Natsuki Komoda, Masaya Nogi, Katsuaki Suganuma, Kazuo Kohno, Yutaka Akiyama, Kanji Otsuka, Nanoscale, 4, 3148 (2012).

[39] Natsuki Komoda, Masaya Nogi, Katsuaki Suganuma, Hirotaka Koga, and Kanji Otsuka , 12th IEEE Int. Conf. on Nanotechnol. (IEEE-NANO 2012).

[40] G.A. Casula, G. Montisci and G. Mazzarella, IEEE Antennas and Wireless Prop. Lett. 12, 1400 (2013).

[41] N. A. Tran, H. N. Tran, M. C. Dang, E. F. Blanc, Adv. Nat. Sci.: Nanosci. Nanotechnol. 1, 2043 (2010)

[42] D. Betancourt, J. Castan, Prog. Elect. Res. C 38, 129 (2013).

[43] C. A. Balanis, Antenna Theory Analysis and Design, 3rd ed. (John Wiley & Sons, 2005).

[44] T. C. Edwards, Foundations for Microstrip Circuit Design, 2nd Ed. (John Wiley & Sons, 1991.

[45] S. L. Zuo, Z. Y. Zhang, J. W. Yang, IEEE Antennas and wireless Propag. Lett. 12, 27 (2013).

[46] http://www.sigmaaldrich.com/catalog/product/aldrich/796042

[47] Arkaprovo Das, Sayantan Dhar and Bhaskar Gupta, 11th IEEE Mediterranean Microwave Symposium (MMS), At Hammamet, Tunisia, MMS-2011, 21 (2011)

[48] K.C. Gupta, R. Garg, I. Bahl, P. Bhartia, 2nd Ed. (Artech House Publishers, 1996).

[49] S. A. Mitilineos and C. N. Capsalis, IEEE T Antenn Propag 55 (9), 2502 (2007).

[50] M. L. Scarpello, D. Kurup, H. Rogier, D. Vande Ginste, F. Axisa, J. Vanfleteren, W. Joseph, L. Martens, and G. Vermeeren, IEEE T Antenn Propag 59 (10), 3556 (2011).

[51] L. Wang, Y. X. Guo, B. Salam, and C. W. A. Lu, presented at the Antennas and Propagation (APCAP), 2012 IEEE Asia-Pacific Conference on, 2012 (unpublished).

[52] T. W. Koo, D. Kim, J. I. Ryu, H. M. Seo, J. G. Yook, and J. C. Kim, IEEE Antennas and Wireless Propagation Letters 10, 1010 (2011).

[53] Bob, (2015), Vol. 2015.

[54] Tran Nhan Ai, Tran Huy Nam, Dang Mau Chien, and Fribourg-Blanc Eric, Adv in Natural Sciences: Nanoscience and Nanotechnology 1 (2), 025016 (2010).

[55] R. Zichner and R.R. Baumann, Adv Radio Sci 9, 401 (2011).

[56] Arshad Hassan, Shawkat Ali, Jinho Bae, and Chong Hyun Lee, Applied Physics A 122 (8), 1 (2016).

[57] G. A. Casula, G. Montisci, P. Maxia, G. Valente, A. Fanti, and G. Mazzarella, IEEE Antennas and Wireless Propagation Letters 15, 1333 (2016).

[58] S. Ali, J. Bae, C. H. Lee, K. H. Choi and Y. H. Doh, Sens and Actuators B: Chemical 220, 634 (2015).

[59] T. Kawashima, H. Matsui and T. Tanabe, Thin Solid Films 445, 241 (2003).

[60] N. Guan, H. Furuya, K. Himeno, K. Goto and K. Ito., IEICE Trans Commun E90-B, 2219 (2007).

[61] D-H. Kim, M-R. Park, H-J. Lee and G-H. Lee, Appl Surf Sci 253, 409 (2006).

[62] M. Ait Aouaj, R. Diaz, A. Belayachi, F. Rueda and M. Abd-Lefdil, Mater Research Bulletin 44, 1458 (2009).

[63] P. Adrian, D. V. Morgan, M. P. Richard, O. J. Martin and P. E. Peter, J. of Appl Physics 95, 4734 (2004).

[64] A. Yabuki and N. Arriffin, Thin Solid Films 518, 7033 (2010).

[65] B. S. Cook, J. R. Cooper, S. Kim, and M. M. Tentzeris, presented at the 2013 IEEE MTT-S International Microwave Symposium Digest (MTT), 2013 (unpublished).

[66] B. S. Cook, J. R. Cooper, and M. M. Tentzeris, IEEE Microwave and Wireless Components Letters 23 (7), 353 (2013).

[67] Hofmann, G. Fischer, R. Weigel, and D. Kissinger, IEEE Transactions on Microwave Theory and Techniques 61 (5), 2195 (2013).

[68] K. Grenier, D. Dubuc, T. Chen, F. Artis, T. Chretiennot, M. Poupot, and J. J. Fournié, IEEE Transactions on Microwave Theory and Techniques 61 (5), 2023 (2013).

[69] K. Grenier, D. Dubuc, P. E. Poleni, M. Kumemura, H. Toshiyoshi, T. Fujii, and H. Fujita, presented at the 2009 IEEE MTT-S International Microwave Symposium Digest, 2009 (unpublished).

[70] K. Grenier, D. Dubuc, P. E. Poleni, M. Kumemura, H. Toshiyoshi, T. Fujii, and H. Fujita, IEEE Transactions on Microwave Theory and Techniques 57 (12), 3246 (2009).

[71] S. P. Parker, McGraw-Hill Dictionary of Scientific and Technical Terms. (McGraw-Hill Education, 2003).

[72] S. K. Pavuluri, R. Lopez-Villarroya, E. McKeever, G. Goussetis, M. P. Y. Desmulliez, and D. Kavanagh, Journal of Physics: Conference Series 178 (1), 012009 (2009).

[73] K. F. E, (Google Patents, 1968).

[74] B. S. Cook, J. R. Cooper, and M. M. Tentzeris, IEEE Transactions on Microwave Theory and Techniques 61 (12), 4714 (2013).

[75] K. Ling, M. Yoo, W. Su, K. Kim, B. S. Cook, Manos M. Tentzeris, and S. Lim, Opt. Express 23 (1), 110 (2015).

[76] S. B. Liao, P. Dourmashkin, and J. Belcher, Introduction to Electricity and Magnetism: MIT 8.02 Course Notes. (PRENTICE HALL, 2011).